DOI: 10.1070/RCR4803

Nanostructured silver sulfide: synthesis of various forms and their application

Stanislav I. Sadovnikov, Andrey A. Rempel, Aleksandr I. Gusev

Institute of Solid State Chemistry, Ural Branch of the Russian Academy of Sciences
ul. Pervomayskaya 91, 620990 Ekaterinburg, Russian Federation

The results of experimental studies on nanostructured silver sulfide are analyzed and generalized. The influence of small particle size on nonstoichiometry of silver sulfide is discussed. Methods for the synthesis of various forms of nanostructured Ag_2S including nanopowders, stable colloidal solutions, quantum dots, core – shell nanoparticles and heteronanostructures are described. The advantages and drawbacks of different synthetic procedures are analyzed. Main fields of application of nanostructured silver sulfide are considered.
The bibliography includes 184 references.

Contents

1. Introduction 303
2. The crystal structure and nonstoichiometry of silver sulfide phases 304
3. Methods for the synthesis of nanostructured silver sulfide 306
4. Chemical deposition of nanostructured Ag_2S from aqueous solutions 310
5. Advantages and drawbacks of various methods for synthesis of nanostructured silver sulfide 320
6. Applications of nanostructured silver sulfide 322
7. Conclusion 324

1. Introduction

Silver sulfide Ag_2S, along with lead, zinc, copper, cadmium and mercury sulfides,[1–5] belongs to the most in-demand semiconductors.[6,7]

S.I.Sadovnikov. Candidate of Chemical Sciences, Senior Researcher of the Laboratory of Nonstoichiometric Compounds at the Institute of Solid State Chemistry, UB RAS.
Telephone: +7(343)362 – 3034, e-mail: sadovnikov@ihim.uran.ru
Current research interests: synthesis, structure and reactivity of metal chalcogenides, colloidal solutions, nanoparticles, nanostructured materials.
A.A.Rempel. Corresponding Member of the Russian Academy of Sciences, Doctor of Physical and Mathematical Sciences, Head of the same Laboratory, Professor of the Department of Physical Methods and Instruments for Quality Control at the Institute of Physics and Technology, Ural Federal University.
Telephone: +7(343)374 – 7306, e-mail: rempel@ihim.uran.ru
Current research interests: nonstoichiometry, structural defects, order – disorder phase transitions, quantum size effects, nanomaterials, nanotechnologies.
A.I.Gusev. Doctor of Physical and Mathematical Sciences, Professor, Principal Researcher of the Laboratory of Nonstoichiometric Compounds at the Institute of Solid State Chemistry, UB RAS.
Telephone: +7(343)362 – 3523, e-mail: gusev@ihim.uran.ru
Current research interests: nonstoichiometry and ordering in solids, thermodynamics, order – disorder phase transitions, condensed matter in nanocrystalline state.

Received 17 December 2017
Translation: A.M.Raevskiy

Recently, nanostructured silver sulfide has been intensively studied due to its potential for application in optoelectronics, biosensorics and catalysis.[8–11] This is an excellent material for fabrication of heterostructures[12] which can also be used in solar cells,[13] IR detectors,[14–16] resistive switches and nonvolatile memory devices.[17–21] Besides, Ag_2S is promising for solar energy conversion into electricity.[22,23] Silver sulfide nanoparticles exhibit antibacterial activity.[24,25] Preparation of stable individual Ag_2S quantum dots to be used as biomarkers[26,27] and application of nanostructured silver sulfide in production of thermoelectric materials[28] are also of high promise.

The application of semiconducting nanostructured silver sulfide in biology and medicine as biosensor is based on the quantum size effects that influence the optical properties of the material. These effects are immediately related to the dependence of the band gap on the Ag_2S nanoparticle size.

Semiconducting Ag_2S/noble metal heterostructures are treated as candidate materials for application in photocatalysis.[9,29] In particular, this is due to the narrow band gap of silver sulfide (about 0.9 eV).

The great potential of nanostructured silver sulfide is supported by relatively simple synthesis and unique functional physical and chemical properties of the material (semiconductor or ionic conductor behaviour, mechanical and thermal stability) that can be controlled by varying the size of nanoparticles (grains, crystallites). Moreover, the possibility of controlling the electrical and optical properties of nanostructured Ag_2S by varying the size and shape of synthesized nanoparticles underlies its potential benefits in

© 2018 Uspekhi Khimii, Russian Academy of Sciences and Turpion Ltd.

various applications including photovoltaic devices, light-emitting diodes, field-effect transistors, biological visualization, *etc*. The most appropriate methods for the synthesis of nanostructured silver sulfide utilize the 'bottom – up' strategy,[30] which involves the assembly of nanoparticles from atoms and molecules. It seems likely that Ag_2S nanocrystals with controlled size and narrow size distribution can be most efficiently produced *via* chemical synthesis of colloidal solutions.

Prior to discussing methods for the synthesis, as well as structural features and properties of nanostructured silver sulfide, we will touch briefly on the notion 'nanomaterial'.

Materials with an average particle (grain, crystallite) size of at most 100 nm are usually treated as nanocrystalline or nanostructured ones.[31 – 34] Recently, it was proved that if the particle size in a solid becomes smaller than a certain value, the properties of the material can change fundamentally, *i.e*., one deals with quantum size effects.[30, 32, 34 – 38] The threshold particle size corresponding to a jumpwise change in the properties of most available materials varies from 1 to 100 nm. The quantum size effects become more pronounced if the particle size is less than 10 nm. Since this particle size falls on the nanometre length scale, materials characterized by the quantum size effects are called nanomaterials. The particle size in the nanomaterials belongs to the key parameters responsible for the specific properties and fields of application of these systems.

Most nanomaterials are characterized by strong violation of long-range order in their structure and the role of many-particle correlations in the atomic arrangement is played by short-range order. In this connection, the term 'nanomaterial' should be rather understood as nanostructured than nanocrystalline material.

The physicochemical properties of semiconductor nanomaterials are significantly different from those of coarse-crystalline ones.[39, 40] The reasons are as follows:[32, 37]

— the nanoparticle size is comparable with the exciton radius in semiconductors; this influences the electronic, optical, luminescent and other properties of nanomaterials;

— small grain size is responsible for the development of the surface of particles, namely, a decrease in the grain size in a solid from 100 to 1 nm causes the proportion of the surface atoms to increase from 1% to 50%; besides, the surface atoms contribute largely to all properties of matter in the nano state;

— the proper size of nanoparticles approaches the size of molecules.

Semiconductor nanoheterostructures, especially, semiconductor/semiconductor ones including quantum wells, quantum wires and quantum dots, allow one to control the fundamental properties of semiconductors, *viz*. the band gap, effective mass and charge carrier mobility.[36, 40 – 43]

Thus, the notion 'nanostructured material' covers a wide range of objects from colloidal solutions and individual nanoparticles to nanoheterostructures of different dimensionality.

Taking account of this fact, in the text below we will discuss methods for the synthesis, as well as the structure and properties of silver sulfide nanopowders, nanoparticles, colloidal solutions and heteronanostructures. We will also dwell on the results obtained by transmission electron microscopy (TEM), high-resolution transmission electron microscopy (HR TEM), scanning electron microscopy (SEM), energy-dispersive X-ray spectroscopy (EDX), dynamic light scattering (DLS), *etc*. No summary reviews on nanostructured Ag_2S have been published so far. Mention may only be made of a small review [2] on the synthesis and optical properties of silver sulfide nanostructures of different morphology.

Main synthetic methods described here are versatile and can be used to obtain all types of chalcogenides.

2. The crystal structure and nonstoichiometry of silver sulfide phases

Silver sulfide has three polymorphs (Fig. 1) whose structures differ from those of the lead, zinc, cadmium and mercury sulfides that have one (cubic *B*1 type for PbS) or two [cubic sphalerite type and hexagonal (usually) wurtzite-type for ZnS, CdS and HgS] polymorphs in the close temperature intervals. The silver sulfide polymorphs are also structurally different from the copper(I) and gallium(III) sulfides having three polymorphs each (orthorhombic, hexagonal and cubic for Cu_2S; and hexagonal, wurtzite-type and sphalerite-type for Ga_3S_2). Compared to other sulfides a distinctive feature of the crystal structure of

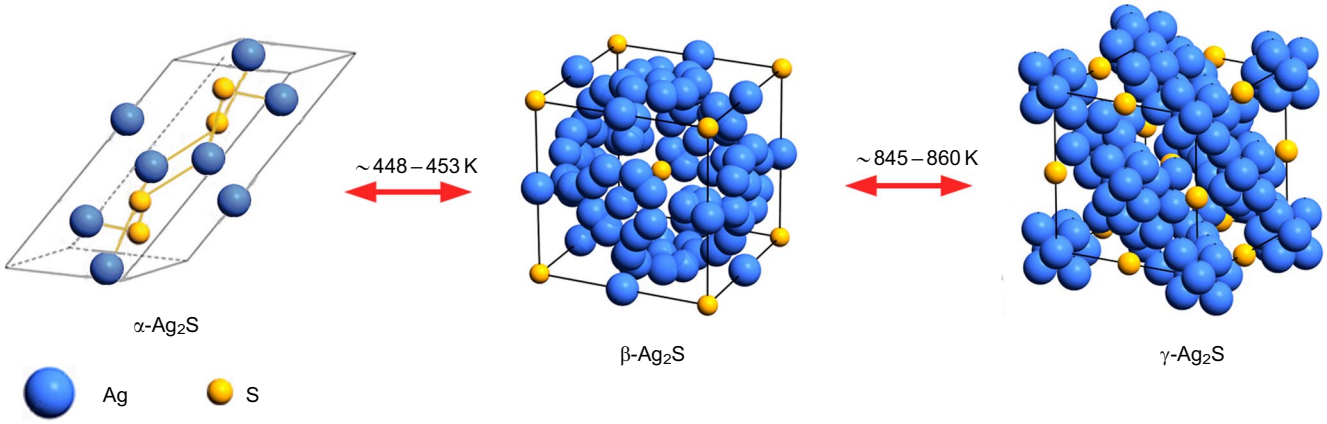


Figure 1. Change in the crystal structure of silver sulfide during reversible phase transitions.[44]
Shown are the unit cells of monoclinic (space group $P2_1/c$) α-Ag_2S (acanthite), cubic (space group $Im\bar{3}m$) β-Ag_2S (argentite) and cubic (space group $Fm\bar{3}m$) γ-Ag_2S.

the silver sulfide phases is that silver atoms are distributed over a very large number of sites in the metal sublattice.

According to the phase diagram of the Ag – S system,[45] silver sulfide has three main polymorphs. The low-temperature semiconducting phase, α-Ag_2S (acanthite), has a monoclinic structure and exists at temperatures below ~450 K. Under equilibrium conditions the cubic phase, β-Ag_2S (argentite), exists in the temperature interval between 452 and 859 K, has a body-centred cubic (*bcc*) sulfur sublattice and exhibits superionic conductivity. The high-temperature cubic phase, γ-Ag_2S, has a face-centred cubic (*fcc*) sulfur sublattice and is stable in the temperature range from about 860 K to the melting point.

It is accepted that the monoclinic phase α-Ag_2S is stoichiometric, whereas the cubic phases β-$Ag_{2\pm\delta}S$ and γ-$Ag_{2\pm\delta}S$ with $\delta \approx 0.02$ are nonstoichiometric and can be either slightly silver-deficient or silver-rich. The homogeneity ranges of the cubic allotropes of Ag_2S were determined.[46–48] It was reported[49] that nonstoichiometric argentite β-$Ag_{2\pm\delta}S$ ($\delta \leqslant 0.002$) exhibits high superionic conductivity ($\sim 1.3 \times 10^3\ \Omega^{-1}\ cm^{-1}$), which is 10^6 times higher than that of the semiconducting monoclinic phase.

Frueh[50] studied the crystal structure of a single crystal of natural mineral acanthite and showed that it has a primitive monoclinic unit cell belonging to the space group $P2_1/n$ ($P12_1/n1$). More recently,[51] it was established that the monoclinic unit cell of α-Ag_2S belongs to the space group $P2_1/c$ ($P12_1/c1$). The lengths and directions of the $a_{P21/c}$ and $b_{P21/c}$ axes coincide with those of the $a_{P21/n}$ and $b_{P21/n}$ axes of the unit cell,[50] while for the $c_{P21/c}$ axis one has $c_{P21/c} = c_{P21/n} - a_{P21/n}$. It is believed[51] that the axes of both acanthite unit cells can be represented as combinations of the a_{bcc}, b_{bcc} and c_{bcc} axes of the *bcc* unit cell of argentite.

Argentite has a cubic unit cell (space group $Im\bar{3}m$) which contains two formula units.[52] Two sulfur atoms occupy the 2(*a*) crystallographic positions and form a *bcc* sublattice. Four silver atoms are distributed with equal probability over 42 positions 6(*b*), 12(*d*) and 24(*h*).

The authors of a single-crystal neutron diffraction study[53] carried out in the temperature range of 459 – 598 K confirmed the cubic structure of β-Ag_2S (space group $Im\bar{3}m$) and essentially refined the distribution pattern of silver atoms. They found that four silver atoms are randomly distributed over 18 positions 6(*b*) and 12(*d*).[53] The occupation probabilities of positions 6(*b*) and 12(*d*) are temperature dependent:

Position	459 K	473 K	533 K	598 K
6(*b*)	0.135	0.110	0	0
12(*d*)	0.266	0.278	0.333	0.333

The temperature 459 K is only 9 K higher than the transition temperature of α-Ag_2S (monoclinic) to β-Ag_2S (*bcc*). One can suggest that the occupation probabilities of positions 4(*e*) by the Ag atoms in the α-Ag_2S structure also differ from unity. In this case, α-Ag_2S can have a nonstoichiometric composition.

In contrast to the results obtained by Cava *et al.*,[53] a high-temperature X-ray diffraction study[54] revealed that four silver atoms in the argentite structure are randomly distributed over 54 positions 6(*b*) and 48(*j*) with an occupation probability of ~0.097 and ~0.0715, respectively.

A model for the structure of cubic (space group $Fm\bar{3}m$) silver sulfide γ-Ag_2S proposed by Frueh[55] assumes that four sulfur atoms occupy the 4(*a*) crystallographic position and form a *fcc* sublattice, while eight silver atoms are randomly distributed over positions 8(*c*) and 32(*f*). Blanton and co-workers[54] used the high-temperature X-ray diffraction data to refine Frueh's model[55] by additionally placing Ag atoms at position 48(*i*). This implies[54] a noticeable silver deficiency in the γ-phase corresponding to nonstoichiometric sulfide $Ag_{1.7}S$.

According to the resuls of the most recent structure refinements of coarse-crystalline acanthite and argentite,[56–60] the low-temperature phase of silver sulfide has the monoclinic acanthite structure and is vacancy-free, thus being stoichiometric, whereas cubic argentite at ~460 K is nonstoichiometric with respect to silver.

Data on possible nonstoichiometry of nanostructured monoclinic acanthite are few. As an example, silver sulfide nanoparticles 5 to 30 nm in size identified in sewage sludge materials were studied.[61] The Ag : S atomic ratio determined from the integrated intensities of the Ag*L* and S*K* lines in the EDX spectrum was 2.1, 1.7 and 1.1 for nanoparticles ~16, ~10 and ~6 nm in size, respectively, *i.e.*, the chemical composition of silver sulfide nanoparticles varied from $Ag_{2.1}S$ ($Ag_2S_{0.95}$) to $Ag_{1.7}S$ ($Ag_2S_{1.18}$) and even to $Ag_{1.1}S$ ($Ag_2S_{1.82}$).[61] The interplanar distance (*d*) in a HR TEM image of nanoparticles was equal to 0.348 nm, thus being rather close to the interplanar distance d_{020} = 0.346 nm in monoclinic silver sulfide with the acanthite structure. The fast Fourier transform (FFT) patterns of the TEM images of silver sulfide nanoparticles in the [100] plane revealed[61] reflections corresponding to the monoclinic phase α-Ag_2S and a number of reflections that were not identified in the monoclinic acanthite structure.

The Ag : S atomic ratio reported[62] for a 17-nm monoclinic silver sulfide nanoparticle was 1.9 : 1, which corresponded to formation of nonstoichiometric sulfide $Ag_{1.9}S$ with a high concentration of vacancies in the silver sublattice.

The structure of Ag_2S nanopowders with an average particle size of at most 45 – 50 nm and possible deviation of their chemical compositions from stoichiometric ones were studied thoroughly[63, 64] along with the structure of coarse-crystalline silver sulfide, which was found to have the monoclinic structure and stoichiometric composition Ag_2S. It was assumed, to a first approximation,[63, 64] that the nanopowder is also stoichiometric and has the same monoclinic crystal structure as the coarse-crystalline silver sulfide. However, the convergence between the experimental and calculated X-ray diffraction patterns in this approximation was poorer than for the coarse-crystalline powder. Minimization involving variation of the occupation probabilities for the crystallographic positions of silver and sulfur atoms led to much better convergence. It was established that the atomic coordinates of Ag and S and the unit cell constants of the silver sulfide nanopowder are close to those of coarse-crystalline Ag_2S. However, the occupation probabilities of the 4(*e*) crystallographic positions by the silver atoms Ag(1) and Ag(2) were smaller than unity, namely, ~0.97 and ~0.96, respectively. It follows that silver sulfide nanoparticles less than 50 nm in size are nonstoichiometric, have the composition ~$Ag_{1.93}S$ and contain vacancies in the metal sublattice. Besides, good Rietveld agreement factors were reported.

Thus, the low-temperature monoclinic phase of nanocrystalline silver sulfide is nonstoichiometric and has the composition $Ag_{2-\delta}S$ with $\delta \leqslant 0.07$.

Under normal conditions, coarse-crystalline silver sulfide with the acanthite structure is a direct-band-gap semiconductor with a wide band gap and low charge carrier mobility. The band gap of α-Ag_2S is temperature-dependent. At 300 K,[65,66] the band gap of acanthite is nearly 0.9 eV (*cf.* 0.9 – 1.1 eV for the commonly accepted value).

The effective masses of an electron and hole in coarse-crystalline acanthite are $m_e = 0.286\,m_0$ and $m_h = 1.096\,m_0$, respectively.[67] Taking account of this fact, the reduced mass of an exciton

$$\mu_{ex} = \frac{m_e m_h}{m_e + m_h} \quad (1)$$

in α-Ag_2S is $\sim 0.23\,m_0 = 2.06 \times 10^{-31}$ kg. The dielectric constant of acanthite (ε) is 5.95.[67] The characteristic size of Wannier – Mott exciton (or the exciton Bohr radius) in a macroscopic semiconductor is given by

$$R_{ex} \approx \frac{n^2 \hbar \varepsilon}{\mu_{ex} e^2} = \frac{n^2 \varepsilon m_0}{\mu_{ex}} a_B \quad (2)$$

where $a_B = \hbar/m_0 e^2 = 0.0529$ nm is the Bohr radius. At $\mu_{ex} = 0.23\,m_0$ and $\varepsilon = 5.95$, for coarse-crystalline acanthite one has $R_{ex} \sim 1.4$ nm for the first exciton state with $n = 1$. The exciton diameter $D_{ex} \approx 2.8$ nm is three- to sixfold larger than the lattice constants of monoclinic acanthite.

3. Methods for the synthesis of nanostructured silver sulfide

Various forms of nanostructured silver sulfide including nanopowders, quantum dots and heteronanostructures are successfully synthesized using hydrochemical bath deposition, template synthesis, sol – gel technique, synthesis in microemulstions, as well as sonochemical, hydrothermal, solvothermal, electrochemical, microwave-assisted synthesis, *etc*. Each method has its advantages and limitations. Many methods are of limited use and allow one to synthesize nanostructured silver sulfide only in the form of, *e.g.*, quantum dots, nanopowders, films or heteronanostructures. The drawbacks of other techniques include poor control of the nanoparticle size during the synthesis, a nonuniform (broad) particle size distribution in the nanomaterials synthesized, multistage character of processes that can involve 3 or 4 stages, utilization of complex instruments, special protective equipment, as well as rare, expensive and hazardous reactants and operation at elevated temperatures.

Silver and other metals are sulfidized using Na_2S,[9,56–58,62–64,68–70] hydrogen sulfide,[71] elemental sulfur dissolved in concentrated NaOH,[72] a solution of hazardous carbon disulfide CS_2 in ethanol,[73–75] sodium thiosulfate,[76] a solution of 3-mercaptopropionic acid in ethylene glycol,[77] thiourea,[78] thioacetamide[79] and their derivatives.

Recently, considerable attention has been paid to the synthesis of various hybrid core – shell heteronanostructures containing silver and its compounds (Ag_2O@Ag_2S, Ag@SiO_2, *etc*.).[80–82] The high surface energy of nanoparticles favours their aggregation. Therefore, when fabricating core – shell nanoparticles, provisions should be made to attach specific groups (organic ligands) to the core surface in order to prevent agglomeration, growth and oxidation of the particles and to obtain stable isolated nanoparticles. Protective shells are prepared using tri-n-octylphosphine oxide (TOPO),[83] L-cysteine,[84,85] glutathione,[21] long-chain amines (hexadecylamine, octylamine, dioctylamine, ethylenediamine),[8] ethylenediaminetetraacetic acid (EDTA) and ethylene glycol.[76] Most of these stabilizing agents are hazardous to health and environment. One of the most in-demand and nontoxic complexing agents providing high degree of electrostatic stabilization is anhydrous sodium citrate (Na_3Cit).[25,56–59,63,64,70,71,86–88] For instance, stable isolated silver sulfide nanoparticles with nontoxic protective carbon-containing citrate shell (Ag_2S@C core – shell nanostructure) were synthesized.[70]

Possible stabilizers for the synthesis of noble-metal (Ag, Au, Pt, Pd) sulfide nanoparticles include extracts from plant raw materials (leaves, seeds, fruits, roots, honey) or aqueous solutions of natural products (royal jelly, wood resin, bovine serum albumin, *etc*.).[89–91] These exotic stabilizers are nontoxic; however, determination of their complex composition still remains an unresolved issue. Therefore, natural stabilizers are of limited use.

According to numerous data, the key role in the formation of Ag_2S nanoparticles is played by complexing agents with sodium citrate being the most important one.†

The term 'controlled deposition' refers to methods that involve the formation of a stable sol from a mixture of the constituent components of the semiconductor. The sol is stabilized using certain stabilizers (*e.g.*, polymers, surfactants) or *via* repulsion from the double electrical layer. The formation of nanoparticles using the sol – gel technique belongs to the methods with controlled deposition.

3.1. Synthesis *via* decomposition of molecular precursors

The synthesis using molecular precursors offers such important advantages as simplicity, safety and compatibility with metal-organic chemical vapour deposition.[92] However, this approach can lead to high selectivity of crystal growth (this cannot be achieved using other synthetic techniques) or to undesired formation of metastable phases.

Injection of an organometallic precursor into a hot solvent is a simple method to prepare particles with specified properties (*e.g.*, highly monodisperse particles of identical shape and size).

An example is provided by a study[8] carried out with silver thiobenzoate as precursor. This compound is stable in air. At room temperature, its crystals decompose in amines to give Ag_2S particles whose size and shape can be controlled by varying the reaction conditions. The most important parameters of the synthesis include the reaction temperature and duration, the type of amine and the relative concentrations of the reactants. It was established[8] that raising the injection temperature to 393 K leads to formation of cube-shaped Ag_2S nanocrystals only. Figure 2 presents their TEM, SEM and HR TEM images. The uniform cubic Ag_2S nanoparticles self-assemble into ordered 2D arrays on the surface of the transmission electron microscope grid (Fig. 2*a*). The average size of these nanoparticles is 44 ± 4 nm. The cubic Ag_2S nanoparticles are single crystals (Fig. 2*c*,*d*).

† Completely harmless standartized food additive E331.

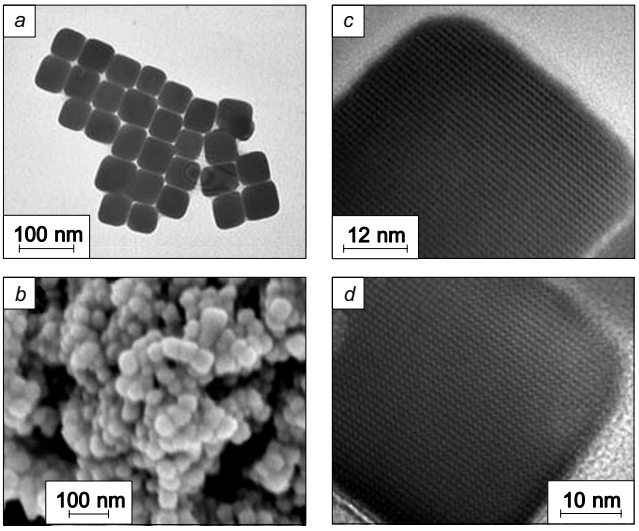


Figure 2. Images of Ag_2S nanocubes produced at 393 K.[8]
A TEM image (*a*), a SEM image of clusters formed by Ag_2S nanocubes (*b*) and HR TEM images of individual nanoparticles (*c*, *d*).

More recently, Ag_2S nanocrystals were obtained[93] using a modified version of the hot injection of the same molecular precursor. Hot injection at 433 K leads to breakdown of Ag – S and S – C bonds in the thiobenzoate molecule and to production of $Ag^{\bullet}$ and $AgS^{\bullet}$ radicals, which are consumed in the formation of Ag_2S nanospheres. As AgS-C(O)Ph is injected into the reaction system pre-heated to 433 K, Ag_2S nanospheres can form even without molecular activators (*e.g.*, alkylamines). Silver sulfide nanocrystallites were prepared[94] by heating silver diethyldithiocarbamate (Ag-DDTC) in air at 473 K for 3 h. The technique is cheap and nontoxic. Monodisperse Ag_2S nanoparticles with controlled size were synthesized[95] by surfactant- and solvent-free thermolysis of nontoxic silver xanthates. The diameter of the Ag_2S nanoparticles was from 8.9 ± 1.2 to 48 ± 4 nm. The particle size was controlled by varying the alkyl chain length in the precursors.

3.2. Synthesis of nanostructured silver sulfide of different morphology

Recently, considerable efforts were made to produce silver sulfide nanoparticles of different morphology and to control the morphology of the semiconductor nanocrystals.[96] Various methods for the synthesis of Ag_2S nanostructures and corresponding mechanisms of formation were studied. For instance, rod-like Ag_2S nanocrystallites were obtained using sodium thiosulfate as the source of sulfur by γ-irradiation of aqueous solutions at room temperature.[97] In this experiment, an important role in the formation of rod-like Ag_2S nanocrystals was played by polyvinylpyrrolidone (PVP). The rod-like Ag_2S nanocrystallites synthesized were 200 to 500 nm in diameter and a few tens of micrometres long, *i.e.*, the aspect ratio was very high (>100). According to X-ray diffraction data, these nanocrystallites comprised nanoparticles $<40-50$ nm in size.

The synthesis of nanostructured Ag_2S using a solution of carbon disulfide in ethanol led to nano- and microstructures of irregular shape only.[98] The growth of Ag_2S nanoparticles in the ethanol – water medium differs from their growth in water or ethanol because the polarities of these media and the solubilities of Ag_2S in them are different. Replacement of water as the reaction medium by the ethanol – water mixture or ethanol causes the morphology of the silver sulfide particles synthesized to change from large nanosheets of irregular shape to leaf-like nanoparticles and ellipsoidal or Y-shaped flakes.

More recently,[99] it was reported that leaf-like Ag_2S nanoparticles (Fig. 3 *a*) were prepared by simple hydrothermal synthesis in a mixture containing a solution of CS_2 in absolute ethanol and an aqueous solution of $AgNO_3$ with NH_3 added. Mixing the two solutions causes the following reactions to proceed:

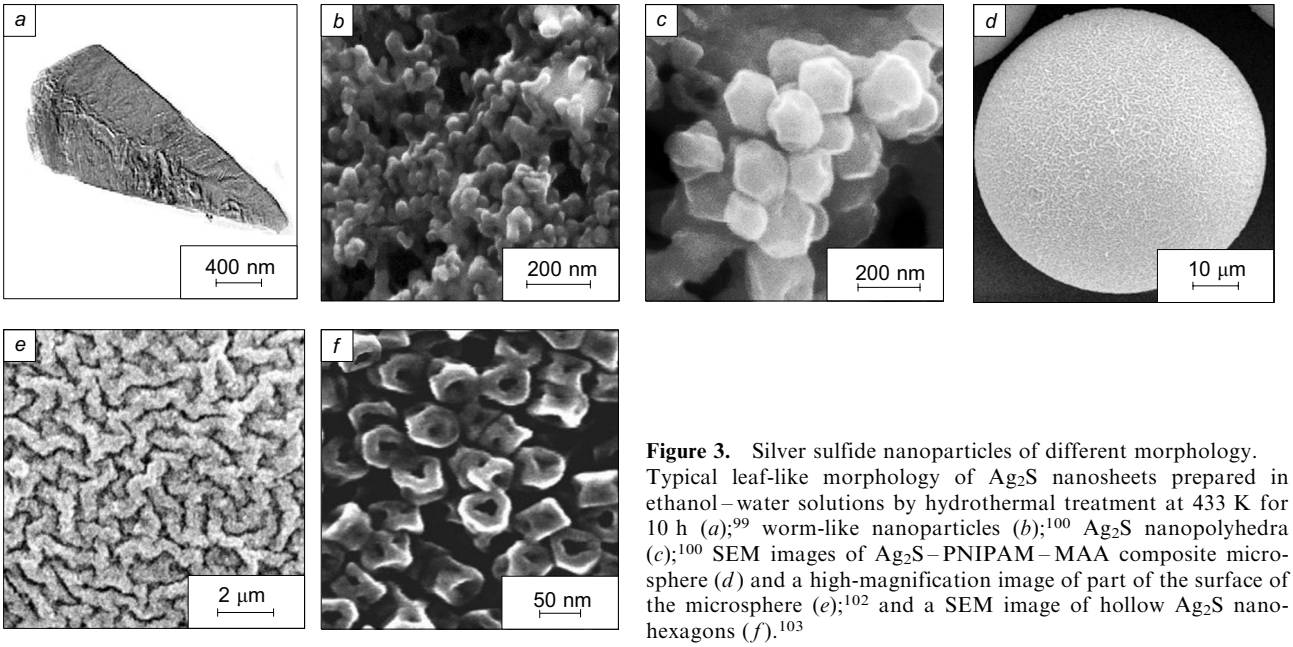


Figure 3. Silver sulfide nanoparticles of different morphology.
Typical leaf-like morphology of Ag_2S nanosheets prepared in ethanol – water solutions by hydrothermal treatment at 433 K for 10 h (*a*);[99] worm-like nanoparticles (*b*);[100] Ag_2S nanopolyhedra (*c*);[100] SEM images of Ag_2S – PNIPAM – MAA composite microsphere (*d*) and a high-magnification image of part of the surface of the microsphere (*e*);[102] and a SEM image of hollow Ag_2S nanohexagons (*f*).[103]

$$2NH_3 + CS_2 \longrightarrow NH_4NHCSSH \quad (3)$$

$$2Ag(NH_3)^+ + NH_4NHCSSH \longrightarrow \quad (4)$$
$$\longrightarrow Ag_2S\downarrow + NH_4SCN + 2NH_4^+$$

Silver sulfide micro- and nanoparticles of different morphology including micrometre-long rod-like crystallites, nanowires and nanopoplyhedra were synthesized in the reaction medium representing a mixture of aqueous solutions of necessary amounts of $AgNO_3$, NH_3 and N_2H_4CS.[100] The size and morphology of Ag_2S particles (Fig. 3 *b*,*c*) can be varied with ease by varying the reactant concentration ratio.

Recently, nanopolyhedra (including sulfide ones) with *fcc* structure have been successfully synthesized.[8, 101] Silver sulfide nanocrystals were synthesized[101] *via* thermolysis of the organometallic precursors $Ag[S_2P(OR)_2]$ ($R = C_nH_{2n+1}$).

The composite microspheres Ag_2S – PNIPAM – MAA and Ag_2S – PNIPAM [PNIPAM is poly(*N*-isopropylacrylamide) and MAA is methacrylic acid] with patterned surface structures were synthesized using a polymeric minigel template method.[102] The minigels were prepared by reverse suspension polymerization of aqueous solutions of corresponding monomers initiated by a solution of ammonium persulfate in n-heptane. The surface structures of the sulfide – polymer composite microspheres depend not only on the nature of the template, but also on the nature of the sulfide. The SEM images of a Ag_2S – PNIPAM – MAA composite microsphere and its surface are shown in Figs 3 *d*,*e*.

Single-crystalline hollow Ag_2S nanohexagons with a narrow size distribution were synthesized in aqueous solutions of $AgNO_3$, $N_2S_2O_3$ and $C_{19}H_{42}BrN$ at 318 K.[103] A SEM image of the hollow Ag_2S nanohexagons is shown in Fig. 3 *f*; hare, parallel edges are separated by a distance of 49 ± 2 nm.

Tetrahedral colloidal Ag_2S nanoparticles were synthesized from aqueous solutions of $AgNO_3$, NH_3 and n-dodecanethiol. The reaction was carried out in an autoclave at 473 K over a period of 5 h.[104] Under the action of van der Waals interactions, highly uniform Ag_2S nanoparticles spontaneously self-assembled into tetrahedral colloidal aggregates representing perfectly ordered 3D superlattice structures (Fig. 4).

Core sulfur nanoparticles are used for the synthesis of hollow Ag_2S nanospheres.[105] The core sulfur nanoparticles were synthesized from sodium thiosulfate in the presence of aqueous solution of cetyltrimethylammonium bromide. As the core formation was completed, aqueous solution of $AgNO_3$ was added. Then, the particles thus obtained were washed with ethanol/water mixture and treated with carbon disulfide for complete conversion of AgBr to Ag_2S and removal of the core to form hollow Ag_2S nanospheres.

Besides, Ag_2S nanoparticles were synthesized[106] by the reaction of $Ag(NH_3)_2^+$ with Na_2S in the presence of polyvinylpyrrolidone using the hydrothermal method. The combined solutions were heat treated in an autoclave at 433 K over a period of 10 h. Well-dispersed Ag_2S nanoparticles had a rice-shaped morphology and most of them were about 70 – 90 long and 30 – 35 nm wide.

Large rice-shaped Ag_2S particles were synthesized using hydrothermal chemical deposition from a mixture of aqueous solutions of silver nitrate (0.05 mol litre^{-1}), sodium sulfide (0.4 mol litre^{-1}) and sodium citrate (0.005 mol litre^{-1}).[56] The reaction mixture was heated in a closed vesel at 373 K at a pressure of $\sim 2 \times 10^5$ Pa for 2 h to give an Ag_2S powder containing small amounts of individual particles about 2000 nm long and about 400 nm wide, as well as large irregular agglomerates.

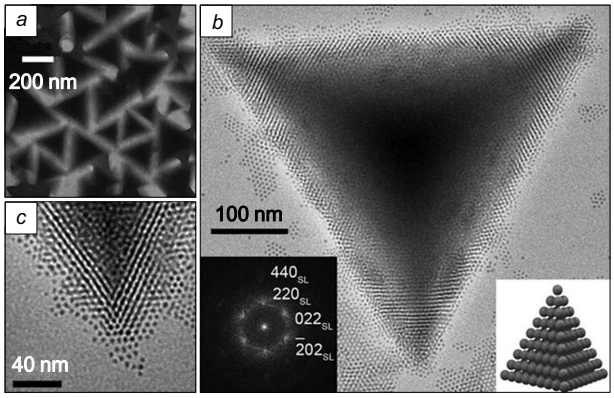


Figure 4. TEM images of tetrahedral colloidal superlattices Ag_2S.[104]
A low-magnification TEM image (*a*); a high-magnification TEM image of an individual tetrahedron (left inset is the fast Fourier transform pattern of the superlattice; the right inset is a scheme of the tetrahedral superlattice of the colloidal crystal) (*b*); and a magnified TEM image of a vertex of the tetrahedron (*c*).

The reasons underlying the formation of silver sulfide nanoparticles of different morphology have not been discussed so far. From the available data it follows that the main methods for the preparation of Ag_2S particles of different morphology include hydrothermal and solvothermal syntheses from weak electrolyte solutions. The nanoparticle growth in solutions from nuclei of the solid phase is due to electrochemical ion transfer from the solution bulk to the surface. As a result, the nucleus surface becomes covered with nonuniformly distributed static charges, the higher charges (larger in absolute value) being observed at the sharp ends, and a potential difference between the nucleus and solution appears.[107] Particles begin to grow at the vertices bearing a negative static charge.[108] Silver cations interacting with sulfur anions attract to the vertices. The nonuniform growth of particles along different crystallographic directions, which is responsible for different morphology, seems to be due to the presence of preferred orientations that can be revealed in the X-ray diffraction experiments.

3.3. Synthesis of Ag_2S nanowires and rod-like nanocrystallites

The one-dimensional (1D) nature of Ag_2S nanowires and rod-like nanocrystallites governs their unique electrical, optoelectronic and mechanical properties. Rod-like nanocrystallites can be to 100 – 200 nm in diameter, while nanowires usually have a bent shape and their diameter is smaller than that of the rod-like nanocrystallites. Nanowires are usually synthesized at high temperatures and(or) using various templates.

Silver sulfide nanowires were successfully synthesized in a simple gas – solid reaction on a silver substrate.[109] A

cleaned silver foil was pre-oxidized and exposed to an $O_2 + H_2S$ atmosphere. The temperature of the reaction system was varied between ambient conditions and 313 K. Silver sulfide nanowires thus obtained were 40 – 150 nm in diameter and up to 100 μm long.

Silver sulfide nanowires were synthesized using anodic aluminium oxide template[17] and by microwave-assisted method.[17, 110]

Yet another experiment[111] involved dissolution of $AgNO_3$ in octadecylamine at 393 K; subsequent addition of sulfur powder led to formation of Ag_2S nuclei. Then, the system was stirred, heated and maintained at 393 K for further growth and crystallization. The process afforded ultralong (up to hundreds of micrometres) Ag_2S nanowires 10 – 30 nm in diameter.

Yan *et al.*[112] prepared Ag_2S nanowires in anhydrous ethanol using a simple template solvothermal method. Typically, a mixture of sulfur powder and $Cd(OAc)_2$ was dissolved in ethylenediamine. The solution was heated in an autoclave at 473 K for 2 h. Then, CdS nanowires thus obtained and $AgNO_3$ were dissolved in anhydrous ethanol and heated in an autoclave at 473 K for 12 h. An excess amount of Ag^+ cations led co complete conversion of CdS nanowires into silver sulfide nanowires.

Cation exchange generated Ag_2S nanowires were also reported.[113]

3.4. Synthesis of Ag_2S nanoparticles and quantum dots using biotechnological and solvothermal methods and thermolysis

Monodisperse water-soluble clusters representing Ag_2S quantum dots coated with ribonuclease-A were synthesized in aqueous phase using a biomimetic method.[114] Ribonuclease-A served as both a stabilizer to prevent aggregation and a biomolecule to modify the surface of Ag_2S nanocrystals in order to reduce toxicity. The Ag_2S nanoparticles had an average size of 5 – 6 nm and a well-defined crystal lattice with clearly seen atomic planes.

Mention was made[115] that biomolecules assisting the formation of inorganic nanostructures favour their electrostatic stabilization and improve their optical properties. To synthesize Ag_2S and Ag_3AuS_2 nanocrystals coated with an L-cysteine (L-Cys) shell, aqueous solutions of silver nitrate and chloroauric acid as well as a solution of L-cysteine in a water/ethylene glycol/ethanol mixture were used. Silver sulfide nanocrystals were prepared using silver nuclei as cores. The scheme of formation of Ag_2S nanoparticles is as follows:[115]

$$Ag^+ + \text{L-Cys} \xrightarrow{298\ \text{K}} [Ag(\text{L-Cys})_n]^+ \quad (5)$$

$$[Ag(\text{L-Cys})_n]^+ + HO^- \xrightarrow{\text{ethanol decomposition, } 343\ \text{K}} \text{L-Cys} - Ag \quad (6)$$

$$\text{L-Cys} - Ag \xrightarrow{\text{C} - \text{S bond dissociation, } 343\ \text{K}} Ag_2S \quad (7)$$

where L-Cys – Ag denotes metallic silver nanoparticles capped with L-cysteine.

Mixing L-cysteine and silver nitrate in ethylene glycol results in a transparent solution, which confirms the formation of metal – cysteine complexes owing to the appearance of Ag^+ – thiol chains.[84] Heating of the solution leads to decomposition of ethanol and formation of metallic silver nanoparticles capped with L-cysteine. Then, the C – S bonds are dissociated and silver sulfide nucleation and growth of Ag_2S nanoparticles occur. The nanoparticles thus prepared were highly uniform in size and interconnected. The size of the Ag_2S nanoparticles varied from 4.3 to 5.8 nm, the average size being 5.2 nm. The biomolecule, *i.e.*, L-cysteine served as the source of sulfur and as stabilizing capping agent, which precludes agglomeration of the sulfide nanoparticles.[115, 116]

Yand and co-workers[117] prepared Ag_2S nanoparticles by pyrolysis using $AgNO_3$ and sulfur powder as precursors and oleylamine acting as a reducing agent and stabilizer during the synthesis. Highly size uniform Ag_2S nanoparticles were obtained by controlling the $AgNO_3$: S ratio and the synthesis duration.

Silver sulfide nanoparticles were synthesized[118] by the solvothermal method in the reaction of $AgNO_3$ with $C_{13}H_{11}NS$ sulfidizer belonging to Schiff bases (azomethines) and various solvents. The synthesis of Ag_2S at 433 K over a period of 12 h with propylene glycol as solvent was chosen as the basic reaction.

Nanostructured Ag_2S was synthesized in the absence of surfactants or in the presence of an anionic sufractant (*e.g.*, sodium dodecylsulfate) or cationic sufractants [*e.g.*, cetyltrimethylammonium bromide and poly(ethylene glycol)]. The surfactants were dissolved in water and(or) in butan-1-ol. Experiments showed[118] that the reaction temperature, the presence of sufractant and the type of solvent affect the size of the Ag_2S nanoparticles. The influence of synthesis conditions on the formation of Ag_2S nanoparticles is illustrated in Fig. 5.

An improved hydro(solvo)thermal method for producing nanostructured silver sulfide was developed.[119] Monodisperse nanocrystals 7.3 nm in size were synthesized in the system containing an ethanol – linoleic acid mixture as the liquid phase, solid silver linoleate and aqueous ethanol solution.

Biocompatible Ag_2S quantum dots were synthesized by thermal decomposition of silver diethyldithiocarbamate with dodecane-1-thiol as covalent ligand and solvent.[120] The reaction mixture was heated to 483 K at a rate of 15 K min^{-1} and kept for 1 h in a nitrogen atmosphere to give hydrophobic dodecanethiol-capped Ag_2S quantum dots with an average diameter of 5.4 to 10.0 nm.

Stable colloidal Ag_2S quantum dots with bright luminescence in the near-IR region were synthesized using 2-mercaptopropionic acid as capping agent.[121] First, 2-mercaptopropionic acid was dissolved in deoxygenated deionized water. Then, $AgNO_3$ was added and the solution was heated to the desired temperature (303, 323 or 363 K). Then, aqueous solution of sodium sulfide was added to the reaction mixture under stirring. The size of Ag_2S nanoparticles could be controlled in the range from 2.3 to 3.1 nm with maximum luminescence emission in the wavelength region of 780 to 950 nm.

A similar one-pot method using 3-mercaptopropionic acid and ethylene glycol was reported in another study.[26] In that case, the surface of the quantum dots was protected with carboxyl groups. The photoluminescence wavelength of the Ag_2S quantum dots can be varied over a wide range from 510 to 1221 nm by varying the growth duration.

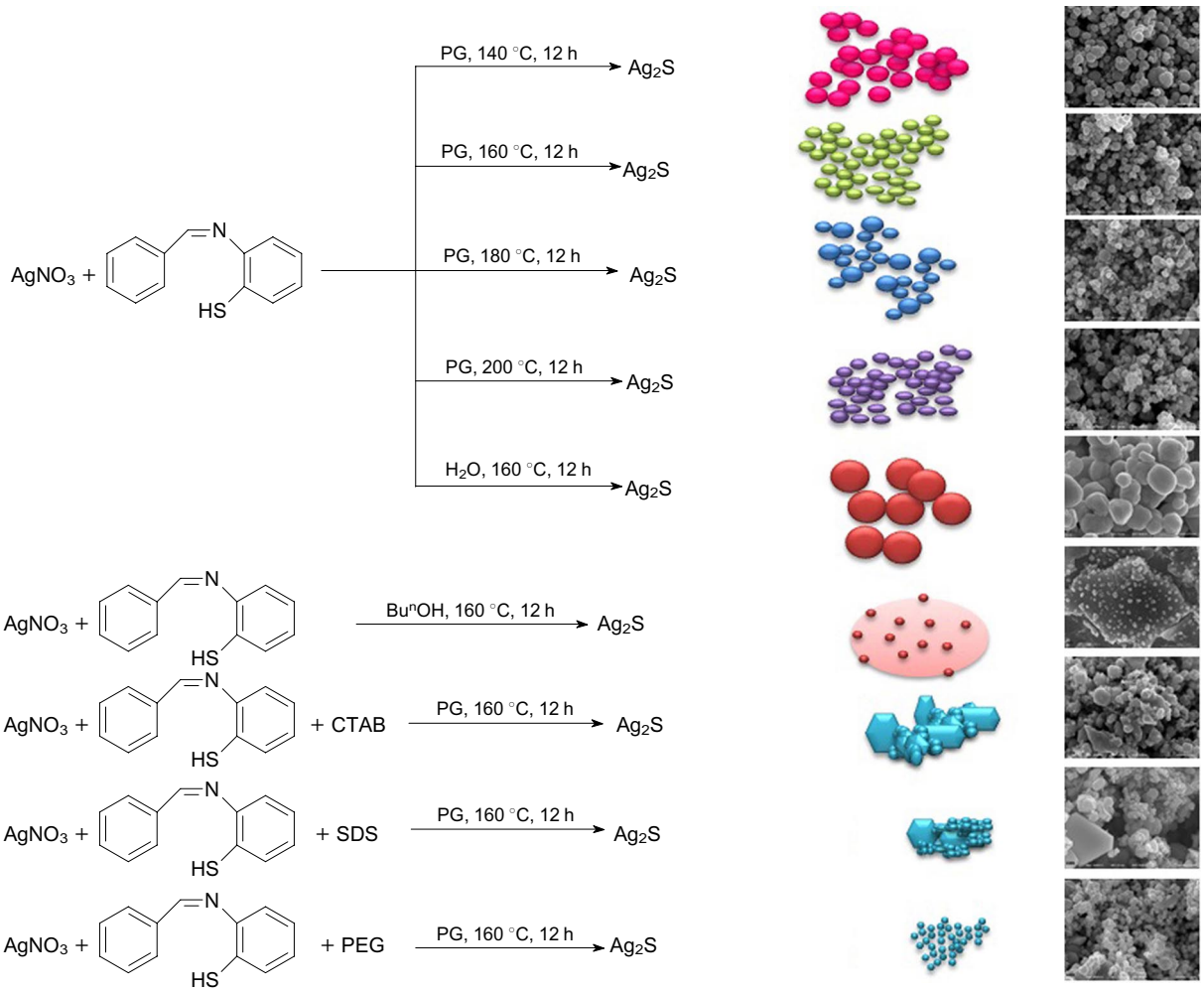


Figure 5. A schematic illustrating the formation of Ag_2S nanoparticles in different conditions.[118]
PG stands for propylene glycol, CTAB stands for cetyltrimethylammonium bromide, SDS stands for sodium dodecylsulfate, and PEG stands for poly(ethylene glycol) 20 000.

4. Chemical deposition of nanostructured Ag_2S from aqueous solutions

Hydrochemical bath deposition (chemical deposition from aqueous solutions) is a well-known method which allows one to synthesize coarse-crystalline and nanocrystalline silver sulfide powders and to prepare colloidal solutions of Ag_2S nanoparticles, isolated shell-protected Ag_2S nanoparticles and various heteronanostructures based on Ag_2S.

4.1. Silver sulfide powders

Chemical deposition from aqueous solutions, which is also called chemical condensation, one-pot synthesis in aqueous solutions and hydrochemical bath deposition, is the most widely used method for the synthesis of nanocrystalline sulfide powders.[122, 123]

Usually, nanostructured silver sulfide is obtained by hydrochemical bath deposition from aqueous solutions of silver nitrate and sodium sulfide. The solubility product (K_{sp}) of silver sulfide is very small, being equal to 6.3×10^{-50} at 298 K.[124] Silver sulfide is formed from aqueous solution of $AgNO_3$ and Na_2S in the simple reaction

$$2\,AgNO_3 + Na_2S \longrightarrow Ag_2S\downarrow + 2\,NaNO_3 \qquad (8)$$

where the concentrations of the anions S^{2-} and cations Ag^+ are related as follows: $c_{S^{2-}} = 0.5\,c_{Ag^+}$. Silver sulfide nanoparticles from coarse-crystalline powder to colloidal nanoparticles can be produced by slightly varying the reactant concentration ratio relative to the ideal reaction (8), by introducing complexing agents and by varying the synthesis conditions.

A generalized scheme for the synthesis of various forms of nanostructured Ag_2S and Ag_2S/Ag heteronanostructures is shown in Fig. 6.

The most widely used complexing agents include solutions of ethylenediaminetetraacetic acid disodium salt (Trilon B) or sodium citrate.

Hydrochemical bath deposition of Ag_2S nanopowders using Trilon B and hydrothermal synthesis of Ag_2S powder have been reported.[69] The concentrations of $AgNO_3$ and Na_2S in different reaction mixtures were 50 and 25 mmol litre^{-1}, respectively; the concentration of Trilon B was varied from 35 to 50 mmol litre^{-1}. To a solution of silver nitrate, Trilon B was added under continuous stirring. Then, this solution was mixed with a solution of sodium

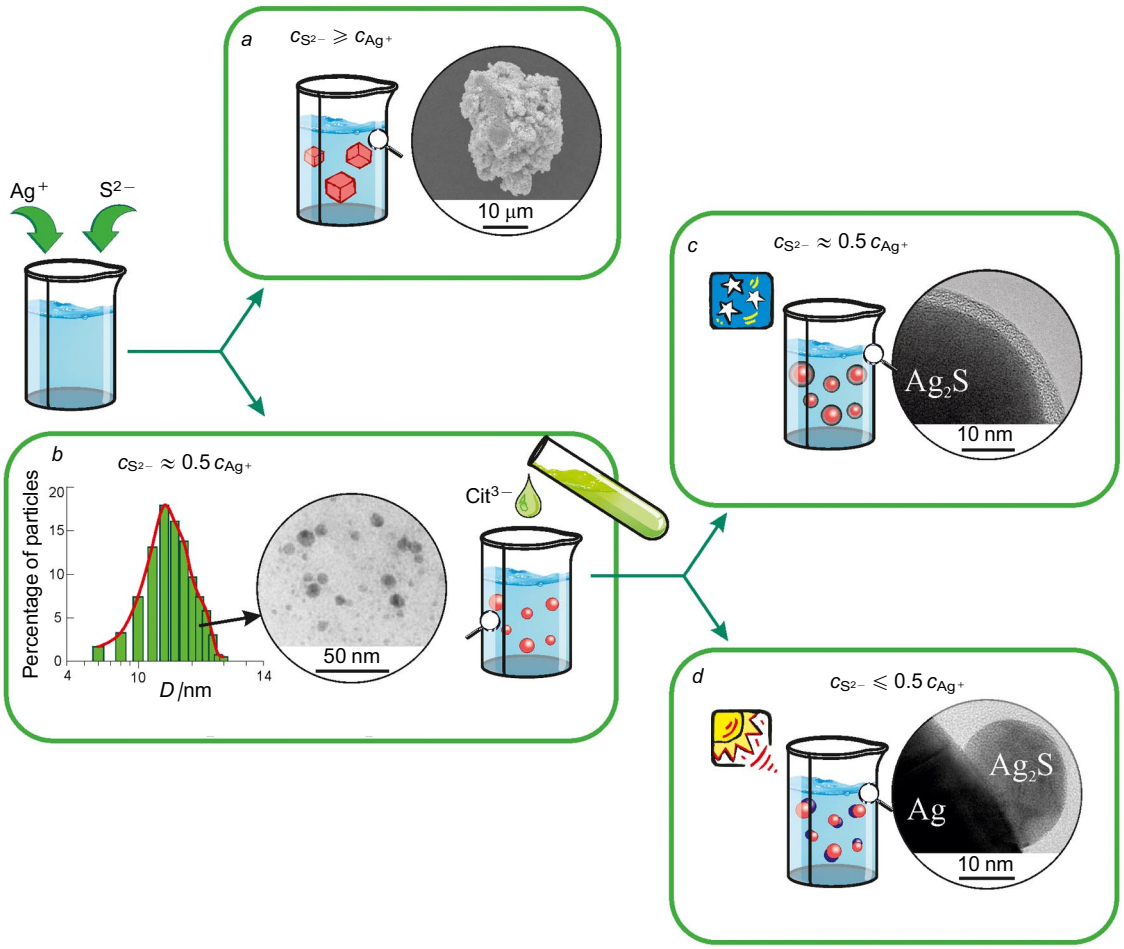


Figure 6. Generalized scheme for the synthesis of various forms of nanostructured silver sulfide.[122] Coarse-crystalline Ag_2S powder (*a*); Ag_2S quantum dots (*b*); Ag_2S@C 'core – shell' nanoparticles with carbon-containing citrate shell (*c*); and Ag_2S/Ag heteronanostructures (*d*). *D* is the nanoparticle diameter.

sulfide, and sulfide formation occurred immediately. All nanoparticles precipitated over a period of two days.

The average size of silver sulfide nanoparticles in the deposited Ag_2S nanopowder evaluated from the broadening of non-overlapping diffraction reflections was 58 ± 8 and 59 ± 8 nm. Based on the specific surface area determined by the Brunauer – Emmett – Teller (BET) method, the size of silver sulfide nanoparticles deposited from the reaction mixtures containing 35 and 50 mmol litre^{-1} of Trilon B was 60 ± 5 and 63 ± 5 nm, respectively. Thus, an increase in the Trilon B concentration in the reaction mixture causes deposition of larger Ag_2S particles. According to BET data, the particle size in coarse-crystalline Ag_2S powder was 975 ± 15 nm.

An EDX analysis showed that, within the limits of experimental error, silver sulfide nanopowders deposited in the presence of Trilon B contain 89.4 ± 0.4 mass % Ag and 10.6 ± 0.1 mass % S. The content of silver in these powders exceeds its possible content in stoichiometric sulfide Ag_2S. It follows that the excess silver exists as an impurity phase in the nanopowders synthesized. Indeed, the X-ray diffraction patterns of the nanopowders deposited in the presence of Trilon B exhibited weak diffraction reflections of Ag. An increase in the concentration of Trilon B in the reaction mixtures from 35 to 50 mmol litre^{-1} is accompanied by increasing the amount of silver impurity in the nanopowders from 3.0 mass % to 4.5 mass %. No metallic silver impurity was detected in coarse-crystalline silver sulfide powder prepared by the hydrothermal method.

The drawbacks of the chemical deposition of silver sulfide from aqueous solutions of $AgNO_3$, Na_2S and Trilon B include the large size of the nanoparticles produced and the presence of considerable amounts of metallic silver impurity.

Coarse-crystalline Ag_2S powder was prepared by hydrothermal synthesis from the reaction mixture containing aqueous solutions of $AgNO_3$ (50 mmol litre^{-1}), Na_2S (400 mmol litre^{-1}) and Na_3Cit (5 mmol litre^{-1}) followed by heating the mother liquor with the precipitated powder in a closed vessel at 373 K over a period of 2 h. The air pressure and the saturated vapour pressure over the solution reached a value of about 2.1×10^5 Pa. It was reported that all silver sulfide powders synthesized had the monoclinic acanthite structure.[69]

Hydrochemical bath deposition using sodium citrate is a simple, reliable, versatile and environmentally safe method for preparation of nontoxic colloidal solutions of Ag_2S nanoparticles, isolated Ag_2S nanoparticles with protective

shells, Ag_2S/Ag heteronanostructures, as well as nano- and coarse-crystalline silver sulfide powders. Usually, dilute aqueous solutions of $AgNO_3$, which possess antibacterial properties and are widely used in pharmacology and medicine, are utilized as the source of silver ions. Emphasize that all forms of nanostructured silver sulfide can be prepared from the same chemical reactants by varying only their concentrations in solutions and the synthesis conditions. A great advantage of hydrochemical bath deposition over other methods is reproducibility of results.[122]

Hydrochemical bath deposition of nanostructured Ag_2S using sodium citrate is an example of a green chemistry method. By definition, green chemistry is the 'design of chemical... processes to reduce or eliminate the use and generation of hazardous substances'.[123] Indeed, hydrochemical bath deposition allows one to obtain valuable products from nontoxic substances using environmentally safe techniques.

This method was utilized [122] for the synthesis of various forms of Ag_2S nanoparticles from aqueous solutions of silver nitrate and sodium sulfide, which served the as sources of Ag^+ and S^{2-} ions with sodium citrate as complexing agent and electrostatic stabilizer.

Coarse-crystalline Ag_2S powder is prepared by hydrothermal synthesis from the reaction mixture containing aqueous solutions of $AgNO_3$, Na_2S and Na_3Cit followed by heating the mother liquor with the precipitated powder in a closed vessel at elevated temperature and pressure.

Coarse-crystalline silver sulfide almost immediately precipitates from an aqueous solution of $AgNO_3$ and Na_2S containing an excess concentration of S^{2-} ions ($c_{S^{2-}} \geqslant c_{Ag^+}$) without adding the complexing agent (see Fig. 6 *a*). If the concentration of S^{2-} ions is high enough or differs only slightly from that necessary to bind all silver ions, *i.e.*, $c_{S^{2-}} \approx 0.5\, c_{Ag^+}$, the addition of sodium citrate to the solution promotes the formation of silver sulfide nanoparticles (see Fig. 6 *b*). Deposition of silver sulfide occurs in a neutral medium (at pH 7).

In aqueous solutions of $AgNO_3$ and Na_2S, sodium citrate plays a triple role. First, it is a complex-forming agent during the deposition of Ag_2S nanoparticles, which occurs both in the light and in the dark. Second, if deposition proceeds in the dark, Na_3Cit is adsorbed on silver sulfide nanoparticles, thus precluding their agglomeration. In this case, increased duration of the deposition process and utilization of reaction mixtures with higher concentrations of Na_3Cit lead to formation of a protective citrate shell on the surface of Ag_2S nanoparticles (see Fig. 6 *c*). Third, if deposition in aqueous solutions with reduced concentration of S^{2-} ions occurs under photoirradiation conditions, sodium citrate can reduce Ag^+ ions to metallic silver.[125] In this photochemical process, citrate ions ($C_6H_5O_7^{3-}$) reduce the Ag^+ cations present in the solution to metallic silver and undergo transformation into $C_5H_4O_5^{2-}$ ions.

$$C_6H_5O_7^{3-} + 2\,Ag^+ \xrightarrow{h\nu} C_5H_4O_5^{2-} + CO_2 + H^+ + 2\,Ag\downarrow \qquad (9)$$

By choosing the concentrations of $AgNO_3$, Na_2S and Na_3Cit in the initial solution provided that the condition $c_{S^{2-}} \leqslant 0.5\, c_{Ag^+}$ is met, one can deposit silver nanoparticles along with Ag_2S nanoparticles and synthesize Ag_2S/Ag heteronanostructures (see Fig. 6 *d*).

Citric acid ‡ is also a possible complex-forming agent for Ag^+ ions; however, its application in the synthesis of silver sulfide leads to undesired shift of the equilibrium towards the acidic region.

Coarse-crystalline powders (about 100 – 1000 nm in size) of stoichiometric silver sulfide with the acanthite structure were synthesized from aqueous solutions of $AgNO_3$ and Na_2S with large excess of sodium sulfide either in the absence or in the presence of sodium citrate at room temperature in the dark.[56, 122]

Powders of silver sulfide nanoparticles were prepared from aqueous solutions of $AgNO_3$ ($c_{AgNO_3} = 50$ mmol litre^{-1}) and Na_2S ($c_{Na_2S} = 0.5\, c_{AgNO_3} + \delta$, where $\delta = 0.5$ mmol litre^{-1}).[63, 122] The concentration of sodium citrate in the initial reaction mixtures was 12.5, 25 and 100 mmol litre^{-1}. A small excess of Na_2S is necessary for the synthesis of silver sulfide containing no impurity of metallic silver nanoparticles. The synthesis was carried out in the dark.

The X-ray diffraction patterns of the deposited Ag_2S nanopowders are shown in Fig. 7. A quantitative analysis of the X-ray diffraction patterns showed that the observed set of diffraction reflections corresponds to nanocrystalline nonstoichiometric acanthite α-$Ag_{1.93}S$. The average size of the coherent scattering regions evaluated from the broadening of the nonoverlapping diffraction reflections ($-1\ 0\ 2$), ($1\ 1\ 0$), ($-1\ 1\ 3$), ($-1\ 0\ 4$), ($0\ 3\ 1$) and ($0\ 1\ 4$) was 43 ± 6, 46 ± 8 and 49 ± 8 nm, respectively. Within the limits of experimental error the size of the coherent scattering regions determined from X-ray diffraction data agree with the particle size evaluated from the BET and DLS data. Silver sulfide nanoparticles were also studied by TEM and SEM. Selected areas of the electron diffraction patterns were obtained as the fast Fourier transform patterns of selected areas of the HR TEM images. Then, inverse fast Fourier transform of the selected diffraction reflections in the HR TEM image was performed using the Gatan Microscopy Suite software [126] and the interplanar distances corresponding to these diffraction reflections were determined. A comparison of the interplanar distances thus obtained and the diffraction data [63] confirmed the monoclinic structure of the powder nanocrystals. According to EDX analysis data, the content of silver and sulfur in the samples corresponded to sulfide $\sim Ag_2S$.

Figure 8 *a* presents a panoramic Raman spectrum of Ag_2S nanopowder, which is similar to a published Raman spectrum of silver sulfide.[127] The Raman spectrum of α-Ag_2S nanopowder in the low-frequency region (210 – 260 cm^{-1}) is smeared and broadened. For more detailed analysis, Fig. 8 *b* demonstrates the Raman spectra of α-Ag_2S nanopowder in the low-frequency region, recorded at 25% and 10% of the excitation power.

These spectra exhibit a series of bands in the range of 90 – 260 cm^{-1}, which mainly correspond to Ag – S bonds. This is consistent with the published data,[21, 128, 129] according to which the Raman spectrum of coarse-crystalline acanthite is characterized by strong bands at $\sim$93, $\sim$122, 167 – 188, 225 – 253 and $\sim$430 cm^{-1}. The peak at $\sim$430 cm^{-1} corresponds to the low-temperature monoclinic acanthite α-Ag_2S.[21] A broad band in the range of 210 – 220 cm^{-1} agrees with the results of a study [130] where

‡ Completely harmless standartized food additive E330.

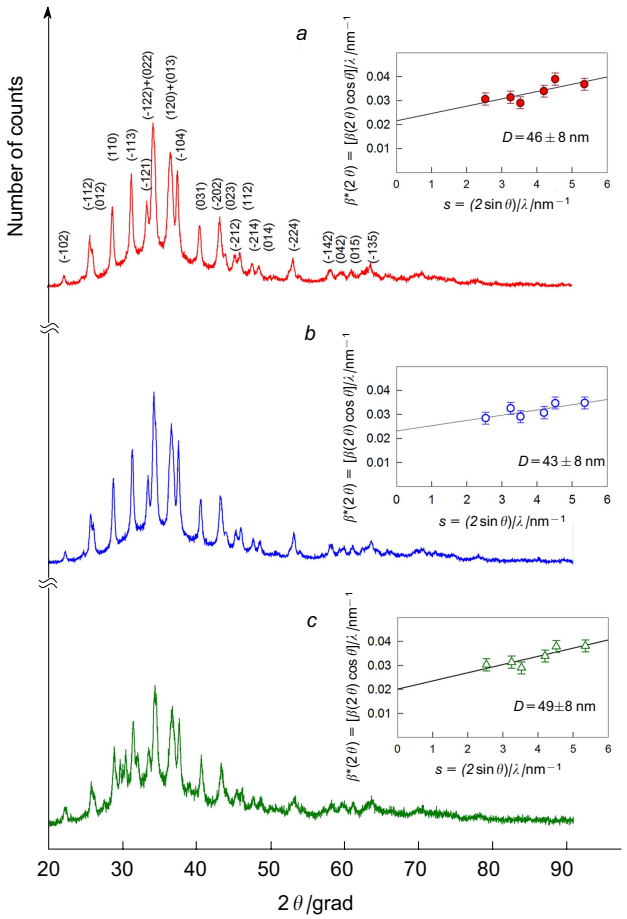


Figure 7. X-Ray powder diffraction patterns of monoclinic Ag_2S nanopowders deposited from the reaction mixtures containing aqueous solutions of $AgNO_3$ (50 mmol litre^{-1}) and Na_2S (25.5 mmol litre^{-1}) at sodium citrate concentrations of 12.5 (*a*), 25 (*b*) and 100 mmol litre^{-1} (*c*).[63,122]
The insets present the estimates of the average size of the coherent scattering regions (D) obtained from the dependence of the broadening of the nonoverlapping diffraction reflections $\beta^*(2\theta) = [\beta(2\theta)\cos\theta]/\lambda$ on the scattering vector $s = (2\sin\theta)/\lambda$, where θ is the diffraction angle and λ is the radiation wavelength.

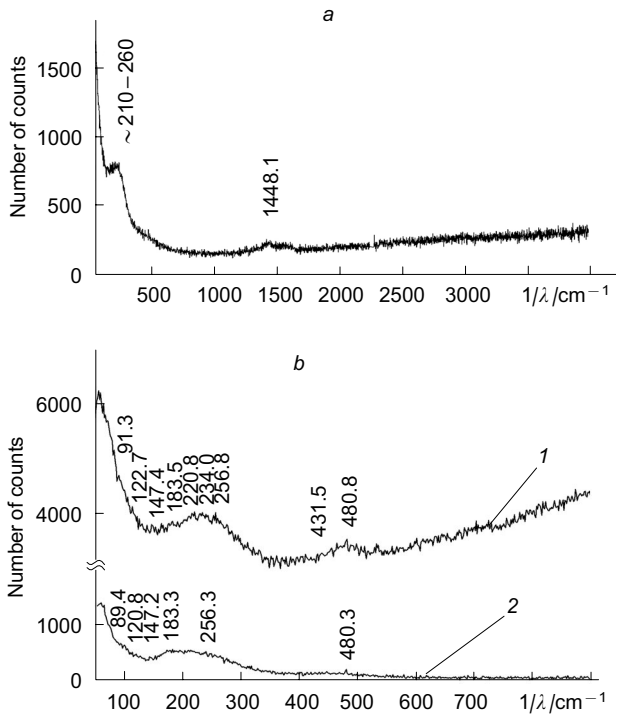


Figure 8. Raman spectra of nanopowder Ag_2S.
Panoramic spectrum (*a*) and Raman spectra in the low-frequency region recorded at 25% (*1*) and 10% (*2*) of maximum power excitation (*b*).

the Raman peak corresponding to Ag_2S nanoparticles was observed near 220 cm^{-1} and with the results of another study.[131] In the acanthite structure, triatomic units Ag – S – Ag are nonlinear and, therefore, the corresponding spectral bands are related to symmetrical longitudinal vibrational modes. In addition to the bands at 93 and 147 cm^{-1} associated with vibrations of the silver sublattice (*i.e.*, phonons), other bands corresponding to symmetrical longitudinal modes (Ag – S – Ag) are allowed and observed. Weak bands at ~220 – 250 and ~430 cm^{-1} can be attributed to first- and second-order longitudinal optical phonon modes, respectively.

A method for the synthesis of Ag_2S nanopowders with specified nanoparticle size by hydrochemical bath deposition was patented.[132]

Silver sulfide nanoparticles in aqueous solutions are formed as a result of interaction of water-soluble silver compounds (mainly $AgNO_3$) with sulfidizers. A sulfidizer containing S^{2-} anions is added to a solution containing Ag^{2+} cations, or sulfide ions are gradually generated in solution during hydrolysis of the sulfidizer (*e.g.*, thiocarbamide). Solid particles that form in the reactions with the sulfidizers that undergo hydrolysis are deposited not only as powder, but also as a film on the substrate surface.[133] An analysis of the deposition kinetics of sulfides including Ag_2S showed[133] that the kinetic curves are S-shaped, which is characteristic of heterogeneous autocatalytic processes occurring on the surface of the solid sulfide phase.

If Ag_2S is deposited, the role of catalyst is played by the surface of silver sulfide formed; the rate of formation of Ag_2S should be proportional to the surface area of the solid phase and to the concentrations of the interacting ions Ag^+ and S^{2-}. Taking account of these facts, the rate of formation of metal sulfide (ω) in aqueous solution with Na_2S as sulfidizer is described by the following model second-order equation

$$\omega = \frac{\mathrm{d}(c_{M0} - c_M)}{\mathrm{d}\tau} = K(c_{M0} - c_M)^{2/3} c_M c_S \qquad (10)$$

where c_{M0} and c_M are the metal ion concentrations in the solution at the initial ($\tau = 0$) and arbitrary ($\tau > 0$) points in time, respectively; K is the rate constant for the reaction; c_{S0} (see below) and c_S are the concentrations of Na_2S at the initial ($\tau = 0$) and arbitrary ($\tau > 0$) points in time, respectively. The amount of sulfide formed in solution during the time interval τ since the beginning of the reaction is proportional to the concentration difference $c_{M0} - c_M = c_{S0} - c_S = x$. To a first approximation, the surface area of the sulfide particles formed (s) is propor-

tional to $(c_{M\,0} - c_M)^{2/3} = x^{2/3}$; therefore, expression (10) can be written as follows:

$$\omega = Ksc_{M}c_S \qquad (11)$$

The formation of crystalline Ag_2S in the thiocarbamide solution proceeds more slowly than in the solution containing sodium sulfide. For instance, the formation of Ag_2S in solutions with Na_2S at room temperature occurs almost immediately, whereas the process in the solutions with N_2H_4CS has an induction period of the order of a few minutes. When using N_2H_4CS, the degree of supersaturation of the solution at the initial instant of deposition is low; therefore, the number of nuclei is relatively small and subsequent hydrolysis of N_2H_4CS leads to the growth of the Ag_2S particles rather than further nucleation of Ag_2S. Thus, hydrolysis of thiocarbamide is the limiting stage of silver sulfide deposition, just like in the case of deposition of other sulfides, *e.g.*, cadmium sulfide.[6] The growth rate of Ag_2S particles is described by Eqn (11), being proportional to the initial reactant concentrations. In the solutions containing N_2H_4CS the growth rate of nuclei of the solid phase is hugher than the nucleation rate; this lads to formation of larger particles compared to the solutions with sodium sulfide.[134]

The kinetics of chemical deposition of Ag_2S by thiocarbamide from aqueous solutions containing $AgNO_3$, Na_3Cit and NH_4OH was analyzed.[135] The measured kinetic curves for silver nitrate conversion to sulfide at different concentrations of Na_3Cit and NH_4OH are typical of heterogeneous autocatalytic processes. A quantitative analysis of experimental data led to the following analytical expression for the rate of formation of Ag_2S:

$$\omega = 1.15 \times 10^4 \left[\exp\left(-\frac{37\,000}{8.31T}\right)\right] s \frac{c_{nit} c_{cit}^{0.3}}{c_{thio}^2 c_{am}^{0.2}} \qquad (12)$$

where c_{nit}, c_{cit}, c_{thio} and c_{am} are the concentrations of $AgNO_3$, Na_3Cit, N_2H_4CS and NH_4OH, respectively. As can be seen, the activation energy for the formation of silver sulfide during the deposition from the solutions studied in Ref. 135 is -37 kJ mol^{-1} and the rate of formation of silver sulfide is proportional to the surface area of the Ag_2S solid phase being formed.

4.2. Colloidal solutions of silver sulfide

Stable silver sulfide colloidal solutions were prepared from reaction mixtures with silver nitrate concentrations varied from 0.3125 to 2.5 mmol litre^{-1} (Table 1) in the dark.[122, 136, 137] The concentration of Na_2S in the reaction mixtures was slightly higher than half the $AgNO_3$ concentration. A small excess of Na_2S ensured the synthesis of silver sulfide colloidal solutions containing no metallic silver nanoparticles as impurity.

The colloidal solutions were characterized by the ζ-potential and by the hydrodynamic diameter of the Ag_2S nanoparticles measured by contactless DLS and obtained from turbidity measurements.

The stability of the colloidal solutions synthesized was confirmed by the fact that their turbidity immediately after the synthesis was equal to zero. The turbidity of the solutions 2, 5, 8, 11, 16, 24, 32, 40, 60 and 100 days after the synthesis was equal to zero.

Table 1. Chemical compositions of reaction mixtures and the average size of silver sulfide quantum dots (D_{DLS}) in colloidal solutions.[122, 137]

Reaction mixture number	Reactant concentrations in the reaction mixture /mmol litre^{-1}			D_{DLS} /nm
	$AgNO_3$	Na_2S	Na_3Cit	
1	0.3125	0.16 + δ	5	2.3 ± 1
2	0.3125	0.16 + δ	2.5	2.7 ± 1
3	0.3125	0.16 + δ	1	3.1 ± 1
4	0.625	0.3125 + δ	5	4.2 ± 2
5	0.625	0.3125 + δ	3.75	5.6 ± 2
6	2.5	1.25 + δ	1	8.0 ±2
7	1.25	0.625 + δ	1.25	8.2 ± 2
8	0.625	0.3125 + δ	2.5	9.2 ±2
9	0.625	0.3125 + δ	1.25	10.0 ± 2
10	2.5	1.25 + δ	2.5	15.0 ± 3
11	0.625	0.3125 + δ	15	16.0 ± 4
12	1.25	0.625 + δ	7.5	17.0 ± 5

Note. δ = 0.01 mmol litre^{-1} (small excess of sodium sulfide Na_2S).

According to DLS data, the size of the Ag_2S nanoparticles in the colloidal solutions studied was at most 20 nm (see Table 1). Such nanoparticles do not precipitate and their size remains almost unchanged. DLS measurements confirmed that the colloidal solutions remain stable over a long period of time. The particle size distribution and the appearance of colloidal solutions containing Ag_2S nanoparticles of different average size are illustrated in Fig. 9 *a*,*b*.

The electrostatic stability of solutions is assessed from the ζ-potential of nanoparticles. The ζ-potential values in the range ±(35 ± 15) mV are indicative of the stability of the colloidal solutions. Particles with higher negative or higher positive surface electric charge are treated as stable.[137] According to the DLS data obtained three days after the preparation of solutions *1*–*12* (see Table 1), their ζ-potentials were in the range between −45 and −28 mV and the nanoparticles were 2–13 nm in size. The ζ-potential and size of the Ag_2S nanoparticles measured 100 days after the preparation of the colloidal solutions remained almost unchanged. Small variations of the ζ-potential and a high negative value of this parameter during long-term storage of these solutions confirm their stability.

Changes in the ζ-potential and in the average size D_{DLS} of quantum dots for the colloidal solutions *1*–*12* determined 100 days after their synthesis are shown in Fig. 9 *c*, namely, D_{DLS} varies between 2 and 17 nm while the ζ-potential varies from −49 to −29 mV (average value is −35 ± 10 mV). It follows that the lower the ζ-potential in absolute value the larger the size of the Ag_2S quantum dots.

Stability studies of silver sulfide colloidal solutions were preceded by additional filtration to remove powders deposited from the reaction mixtures containing $AgNO_3$, Na_2S and Na_3Cit. Figures 10 *a*,*b* present the TEM images of the colloidal solutions containing Ag_2S nanoparticles 15–35 and 12–18 nm in size, respectively. The HR TEM image of

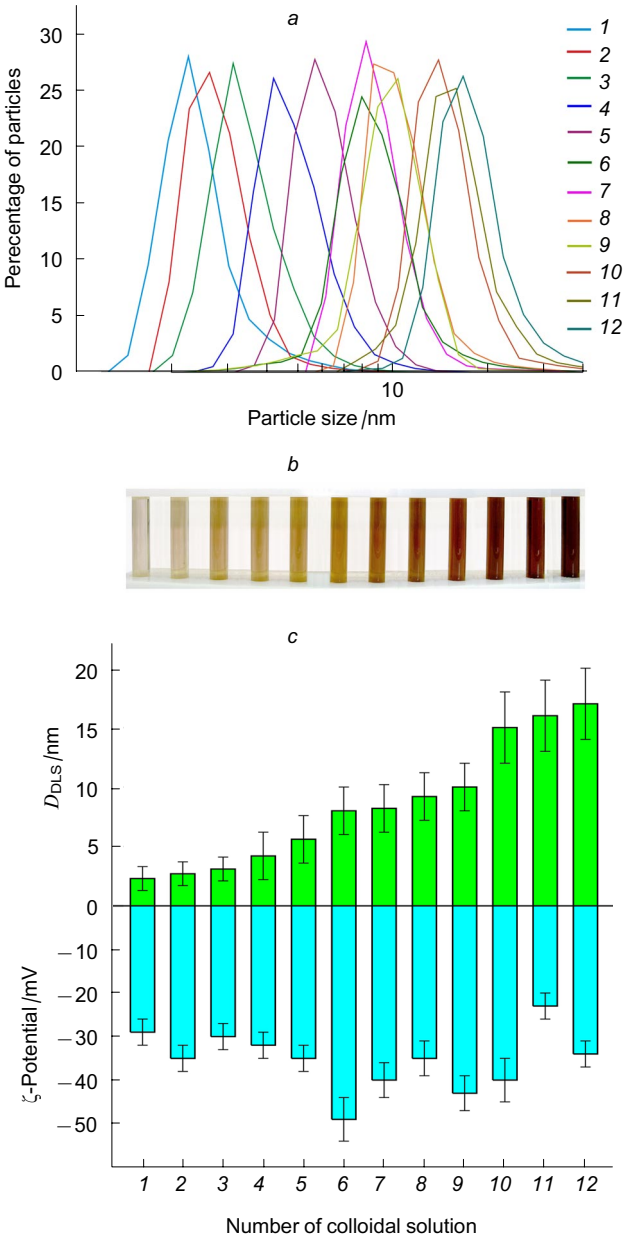


Figure 9. Particle size distributions in colloidal solutions *1* – *12* (see Table 1) obtained from DLS measurements (*a*), appearance of the colloidal solutions (*b*) and average size (D_{DLS}) and ζ-potential (in mV) of Ag_2S quantum dots measured 100 days after the synthesis (*c*).[122]

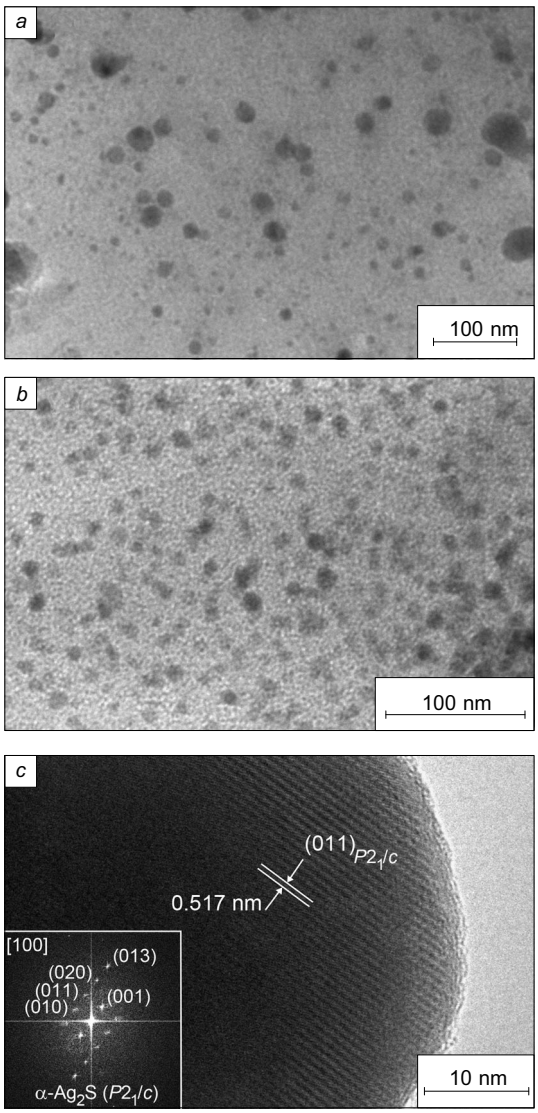


Figure 10. TEM images of colloidal solutions of Ag_2S nanoparticles of different size (*a*, *b*); HR TEM image of monoclinic silver sulfide nanoparticle with acanthite structure and its fast Fourier transform pattern along the [100] zone axis (see inset) (*c*).[136]

an Ag_2S nanoparticle from the colloidal solution shown in Fig. 10 *a* and its FFT pattern are shown in Fig. 10 *c*. The observed diffraction reflections and interplanar distances correspond to monoclinic acanthite.

The results of the DLS measurements in the colloidal solutions[136] made it possible to establish how the particle size depends on the storage time of the solutions.

The particle size in solutions *I* and *II* with the following reactant concentrations (mmol litre^{-1}):

Solution	$AgNO_3$	Na_2S	Na_3Cit
I	50	25.1	25
II	50	25.1	12.5

was measured by DLS immediately after the synthesis. Silver sulfide nanoparticles formed in the solution immediately agglomerated; since agglomerates deposited with time, the size of the particles present in the solution changed.

Initially, bimodal agglomerate size distributions were observed for the solutions. Three days after, most large particles precipitated and the particle size distributions in both solutions became monomodal. Then, the solutions above the precipitates were decanted.

The residues were three times washed with distilled water, aqueous suspension thus obtained was sonicated to break down agglomerates and filtered. The filtrates represented aqueous colloidal solutions of silver sulfide nanoparticles. One day after filtration, filtrates *I* and *II* contained nanoparticles with an average size of 60 ± 10 and 55 ± 10 nm, respectively. The measurements carried out eight days after filtration revealed repeated agglomeration of nanoparticles in the solutions; however, no visible depo-

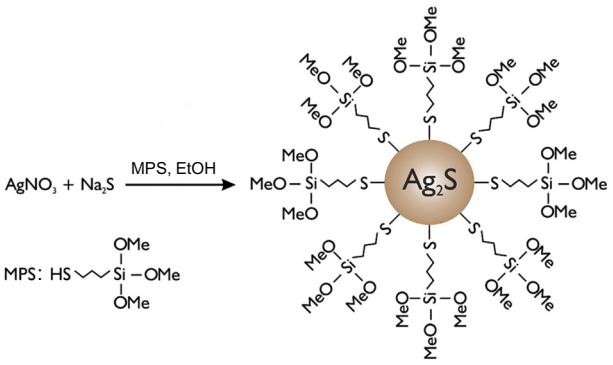


Figure 11. Scheme for the synthesis of water-soluble MPS-terminated Ag_2S nanoparticles.[140]

sition was observed. Probably, the agglomerated Ag_2S particles were in a suspended state, the largest agglomerates precipitated, but their amount was too small to be observed. Deposition was observed visually only 30 days after filtration.

Sixty days after filtration the DLS measurements showed that most particles in both solutions were about 50 nm in size (*cf.* 60 ± 10 and 55 ± 10 nm for the average particle size in solutions *I* and *II*, respectively). The size of the nanoparticles remaining in the aqueous colloidal solution did not change, so the solution was stable over a period of more than three years.

The method of preparation of stable aqueous colloidal solutions of silver sulfide [122, 136] was patented.[138]

Hydrochemical bath deposition was used [139] to synthesize stable water-soluble Ag_2S quantum dots from aqueous solutions of $AgNO_3$, NH_4OH and Na_2S at pH varied from 8.5 to 11.0. The average size of the Ag_2S quantum dots two and seventy days after the synthesis was $\sim 5 \pm 2$ and 33 ± 5 nm, respectively.

The addition of trimethoxy(3-sulfanylpropyl)silane to colloidal solutions to stabilize Ag_2S particles (Fig. 11) allows one to synthesize Ag_2S nanoparticles with a stable average size of about 15 nm.[140]

4.3. Ag_2S@C core – shell nanoparticles

Hybrid core – shell heteronanostructures based on semiconductor compounds of silver (*e.g.*, Ag_2O@Ag_2S, see Ref. 80) make it possible to change the optical properties of semiconductor nanoparticles and to create a protective shell on the nanoparticle surface. Ag_2S@C core – shell nanoparticles with the silver sulfide core and carbon-containing citrate shell were synthesized.[70, 141]

An electron microscopy study of colloidal solutions prepared by chemical deposition from aqueous solutions of $AgNO_3$ and Na_2S without sodium citrate and in the presence of different concentrations of this compound revealed two types of Ag_2S nanoparticles, *viz.*, 'bare' ones and those coated with amorphous carbon-containing citrate shell.

The X-ray diffraction patterns of Ag_2S nanopowders deposited from a mixture of aqueous solutions of $AgNO_3$ (5 mmol litre^{-1}), Na_2S (2.5 mmol litre^{-1}) and Na_3Cit (5 mmol litre^{-1}) are shown in Fig. 12 *a* – *d*. These nanopowders differ in the residence time in solution (from 20 to 1200 min). An analysis of the X-ray diffraction patterns showed that the observed diffraction reflections correspond to nonstoichiometric acanthite $\sim Ag_{1.93}S$.

The TEM images clearly demonstrate that silver sulfide nanoparticles are coated with amorphous shells (Fig. 12 *e* – *h*). Other things being equal, the shell thickness increases with increasing residence time of the nanoparticles in the colloidal solution containing citrate ions and with increasing Na_3Cit concentration in the solution. The interplanar distance values confirmed the monoclinic structure of the colloidal silver sulfide nanoparticles; they are in good agreement with published data [63] on the structure of nanocrystalline nonstoichiometric acanthite α-$Ag_{1.93}S$.

The chemical composition of the core – shell nanoparticles was determined from the results of EDX analysis. Namely, the content of silver and sulfur in the nanoparticles was shown to correspond to sulfide $\sim Ag_{1.93-1.98}S$. In addition to the peaks from silver and sulfur, the EDX spectra exhibit a carbon K_α line whose intensity increases with increasing thickness of the amorphous shell. It follows that one deals with the carbon-containing citrate shell of the sulfide nanoparticle. Indeed, three carboxyl groups of sodium citrate have a high coordination affinity towards silver ions, which favours the attachment of citrate groups to the surface of the silver sulfide nanoparticles and precludes their aggregation. In other words, citrate ions are adsorbed on the nanoparticle surface and form a shell, which hampers the growth and agglomeration of nanoparticles.

A TEM image of an Ag_2S@C core – shell nanoparticle and its schematic representation are presented in Fig. 13. The Ag_2S core nanoparticle about 37 nm in diameter is coated with the carbon-containing shell ~ 3.2 nm thick. The total diameter of the core – shell nanoparticle is ~ 40 nm.

The mechanism of formation of the carbon-containing citrate shell on the Ag_2S core is shown in Fig. 14. In the solutions containing sodium citrate the $C_6H_5O_7^{3-}$ ions are adsorbed on the surface of Ag_2S nanoparticles and form a discontinuous shell. As the residence time of Ag_2S nanoparticles in the solution increases, the bare spots are gradually covered with citrate complexes and thus a continuous C-containing shell is formed. Gradual adsorption of citrate complexes makes the shell surface more smooth and thick.

According to published data,[122, 141] the formation of a shell depends on the concentrations of the silver and sulfur precursors on the one hand and on the sodium citrate concentration on the other hand. If in solution one has $c_{S^{2-}} = 0.5\, c_{Ag^+}$, and $c_{Cit^{3-}} < 0.25\, c_{Ag^+}$, the amount of citrate ions is insufficient to form a continuous citrate shell and a discontinuous nonuniform coating is formed. A continuous shell is formed at $0.25\, c_{Ag^+} \leqslant c_{Cit^{3-}} \leqslant c_{Ag^+}$. If the citrate concentration is high and $c_{Cit^{3-}} \gg c_{Ag^+}$, an amorphous citrate matrix with incorporated nanoparticles about 12 to about 40 nm in size is formed in the solution. By varying the initial reactant concentrations in the reaction mixture and the deposition conditions, one can prepare Ag_2S@C nanoparticles with different Ag_2S core size and different controlled thickness of the nontoxic carbon-containing citrate shell.

Thus, hydrochemical bath deposition allows one to prepare Ag_2S@C nanoparticles with specified core size (from 10 to 50 nm) and shell thickness (from 1.5 to 10 nm). The method for preparation of Ag_2S@C nano-

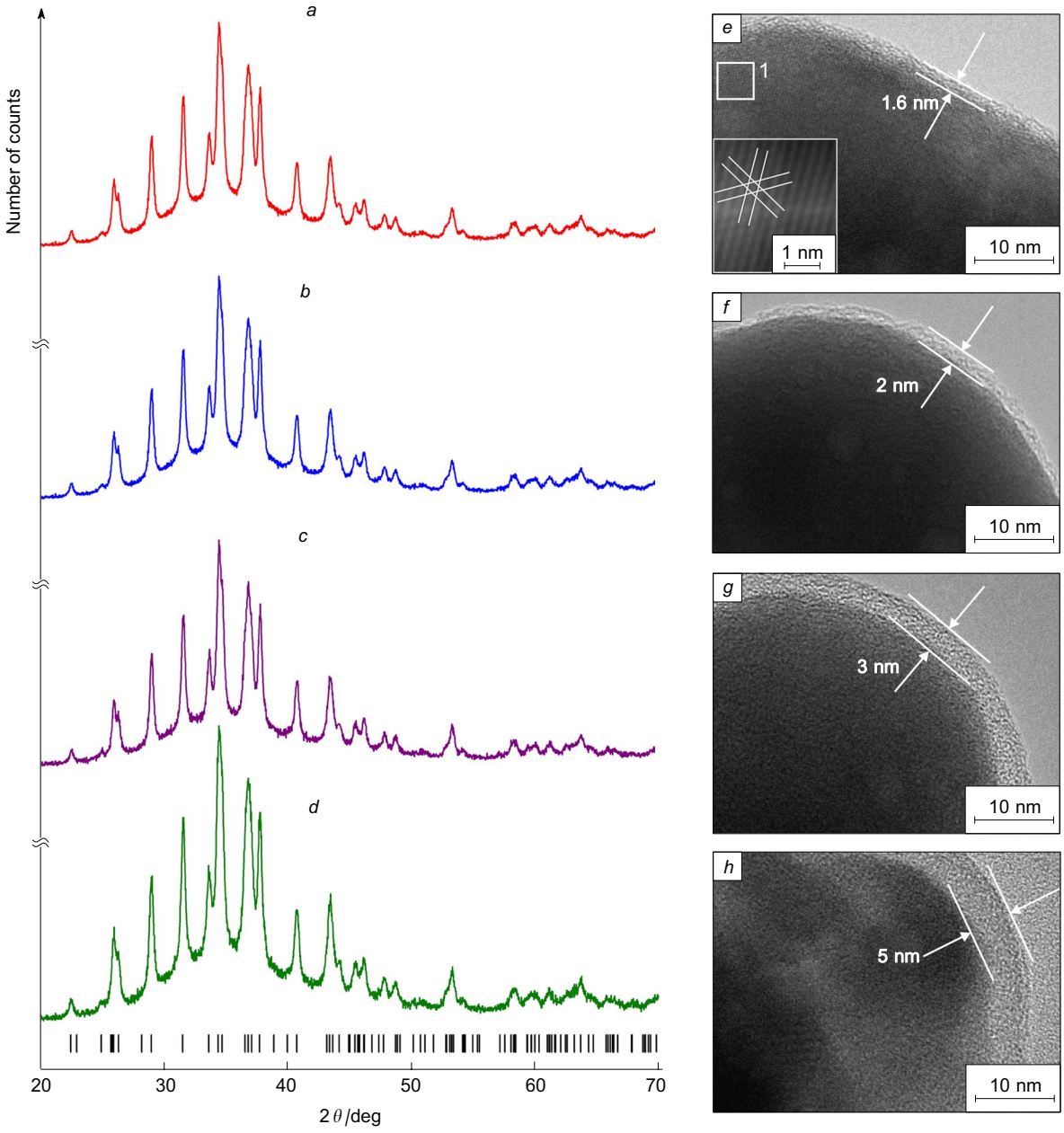


Figure 12. X-Ray diffraction patterns of monoclinic Ag_2S nanoparticles deposited from the reaction mixture containing $AgNO_3$ (5 mmol litre^{-1}), Na_2S (2.5 mmol litre^{-1}) and Na_3Cit (5 mmol litre^{-1}) (*a*–*d*) and the TEM images of Ag_2S nanoparticles with amorphous citrate shell kept in solution over different periods of time (*e*–*h*).[70]
Time /min: 20 (*a*, *e*), 40 (*b*, *f*), 420 (*c*, *g*) and 1200 (*d*, *h*); the lower left inset in Fig. *e* shows a filtered image of region *1*.

particles with protective citrate shell by hydrochemical bath deposition was patented.[142]

4.4. Ag_2S/Ag heteronanostructures

Multifunctional hybrid nanocomposite systems like Ag_2S/Ag heteronanostructures comprising a semiconductor and a noble metal are in high demand.

Hybrid (composite) semiconductor/metal heteronanostructures offer prospects for not only combining, but also controlling the properties of individual components. Owing to synergistic effects resulting from the interaction between the metal and semiconductor the hybrid heteronanostructures can possess improved properties. Possible fields of application of the Ag_2S/Ag heteronanostructures include micro- and nanoelectronics, in particular, production of nonvolatile memory devices and resistive switches.[18, 20, 21, 143 – 145]

The synthesis of Ag_2S/Ag heteronanostructures has been considered in detail[9, 143, 146] and a general scheme of transfer of transition-metal ions from aqueous solutions to the organic phase using ethanol was proposed.

Ag_2S/Ag heteronanostructures were prepared[18] by the electrochemical method using anodic aluminium oxide (AAO) template. Silver nanowires deposited in the porous

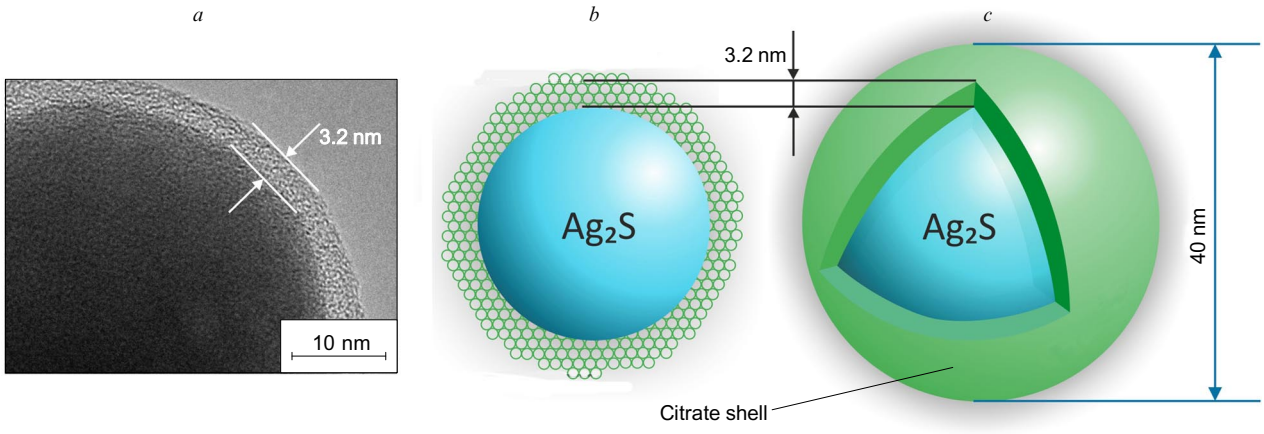


Figure 13. TEM image of Ag_2S@C core–shell nanoparticle (*a*) and a schematic representation (*b*) and section (*c*) of the nanoparticle.[70]

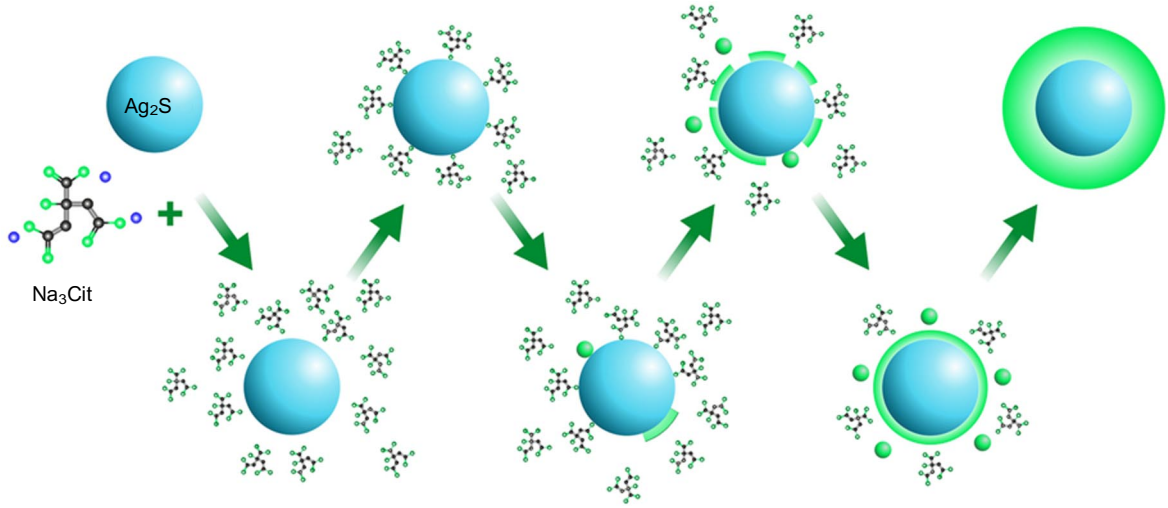


Figure 14. Mechanism of formation of protective citrate shell on Ag_2S core: a schematic.[122]

AAO membrane converted into Ag_2S nanotubes as a result of electrochemical sulfidization.

A method for room-temperature synthesis of Ag_2S/Ag heterodimers was proposed.[25] First, monodisperse CdS colloidal nanospheres were synthesized in poly(ethylene glycol). They were used as solid precursor for further chemical transformation into Ag_2S nanospheres by cation exchange, as well as a template for the deposition of metallic silver. As a result, a tetrahedral Ag nanocrystal grew on each Ag_2S nanosphere.

An extended array of Ag_2S/Ag nanodots was fabricated by sputtering silver onto a silicon substrate using an ultrathin porous AAO membrane template followed by dry sulfidization in H_2S atmosphere at room temperature.[145] The process resulted in the formation of a dense array of bilayer Ag_2S/Ag nanodots with a characteristic size of 45 nm.

A wet chemical process was used[147] to fabricate Ag_2S flat thin films on silver electrodes utilized in fabricating an Ag_2S/Ag atomic switch. Resistive-switching Ag_2S/Ag nanoclusters for memory devices were formed by sulfidization of finely disperse silver films.[21] Silver nanocluster arrays were fabricated by thermal annealing of silver films 10 nm thick at 500 K for 40 min immediately after vacuum thermal evaporation. Low-temperature sulfidization to obtain Ag_2S particles was carried out in hydrogen sulfide atmosphere.

Monodisperse Ag_2S@Ag core–shell nanoparticles were fabricated using laser ablation of an Ag target in an aqueous solution containing thioacetamide and hexadecyltrimethylammonium bromide.[148]

Ag_2S/Ag heteronanostructures were synthesized by deposition from aqueous solutions of $AgNO_3$, Na_2S and Na_3Cit at a reduced concentration of sodium sulfide ($c_{Na_2S} < 0.5\, c_{AgNO_3}$) under irradiation at 450 nm using a light-emitting diode (irradiation power was 15 mW cm^{-2}). The structure and properties of the solutions were studied.[149–152] Such mixtures are characterized by simultaneous occurrence of two processes, namely, the formation of Ag_2S and the formation of silver nanoparticles as a result of photochemical reduction of Ag^{2+} ions by the citrate ions. Under certain synthesis conditions, the Ag and Ag_2S nanoparticles become in immediate contact, thus forming the Ag_2S/Ag nanocomposite. The TEM and SEM images of Ag_2S, Ag and Ag_2S/Ag particles and the corresponding FFT patterns are shown in Fig. 15.

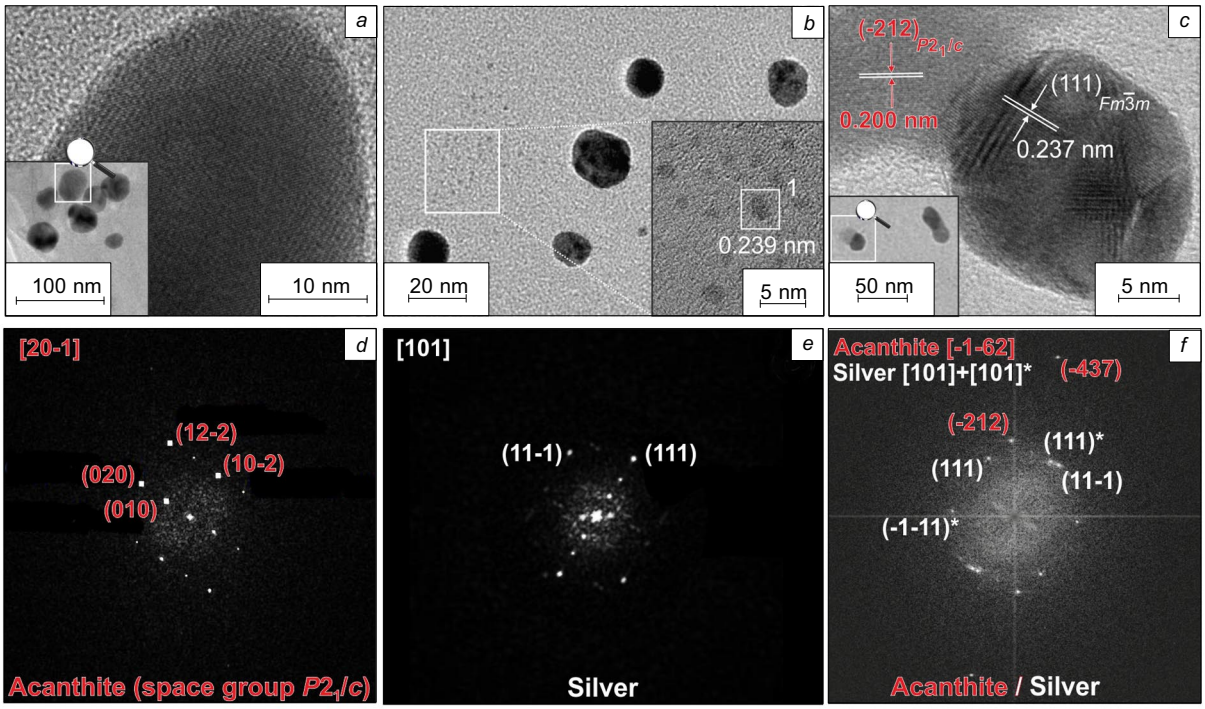


Figure 15. Hydrochemical bath deposition of Ag_2S/Ag heteronanostructures.[150, 151]
TEM images and SEM images (see insets) of Ag_2S (*a*) and Ag nanoparticles (*b*) and Ag_2S/Ag heteronanostructures (*c*); fast Fourier transform patterns of the TEM images shown in Fig. *a*–*c*, respectively (*d*–*f*).

The synthesis was carried out as follows. The complex-forming agent was added to an aqueous solution of silver nitrate in the dark and then an aqueous solution of Na_2S was added. This led to deposition of silver sulfide nanoparticles (see Fig. 15 *a*). Then, the solution was irradiated with monochromatic light at 450 nm. In accordance with the photochemical reaction (9), in aqueous solutions Ag^+ cations are reduced by $C_6H_5O_7^{3-}$ ions to metallic silver nanoparticles (see Fig. 15 *b*). Reduction of silver on the surface of the Ag_2S nanoparticles leads to formation of Ag_2S/Ag heteronanostructures (see Fig. 15 *c*).

The diffraction reflections in the FFT pattern (Fig. 15 *d*) and the interplanar distances for the silver sulfide nanoparticle correspond to monoclinic nanocrystalline acanthite α-$Ag_{1.93}S$.[63] The silver nanoparticle with cubic (space group $Fm\bar{3}m$) structure clearly demonstrates microtwinning along the direction of the (111) planes, which is confirmed by the FFT pattern (see Fig. 15 *e*). The FFT pattern (see Fig. 15 *f*) of the TEM image of the Ag_2S/Ag heteronanostructure (see Fig. 15 *c*) exhibits reflections from monoclinic silver sulfide and twinning reflections from cubic silver. According to EDX analysis data, the contents of Ag (∼86.3 ± 0.4 mass %) and S (∼12.9 ± 0.1 mass %) in the Ag_2S nanoparticle correspond to sulfide $\sim Ag_{1.93-1.98}S$. The Ag nanoparticle contains silver only, while the Ag_2S/Ag heteronanostructure contains Ag (∼87.8 mass %) and S (∼11.5 mass %).

Figure 16 presents a TEM image of a typical Ag_2S/Ag heteronanostructure formed in a colloidal solution resulting from a mixture of aqueous solutions of $AgNO_3$ (50 mmol litre^{-1}), Na_2S (24.5 mmol litre^{-1}) and Na_3Cit (12.5 mmol litre^{-1}). One can see that the Ag_2S and Ag nanoparticles are in immediate contact. The Ag nanoparticle also clearly demonstrates microtwinning along the direction of the (111) planes, confirmed by the FFT pattern of the TEM image. According to EDX analysis data, this nanoparticle contains silver only. The interplanar distances determined for the silver sulfide nanoparticle correspond to monoclinic acanthite. The zone axis of the Ag_2S nanoparticle matrix is $[101]_{P1_{1/c}}$.

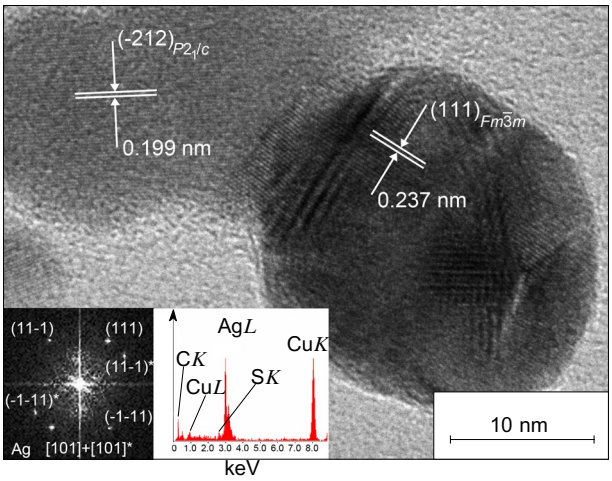


Figure 16. TEM image of Ag_2S/Ag heteronanostructure.[122, 151]
A monoclinic (space group $P2_1/c$) silver sulfide nanoparticle with the acanthite structure (upper left corner) is in contact with the cubic (space group $Fm\bar{3}m$) silver nanoparticle. Lower left insets: a fast Fourier transform pattern of the TEM image of the silver nanoparticle and the corresponding cumulative elemental EDX pattern.

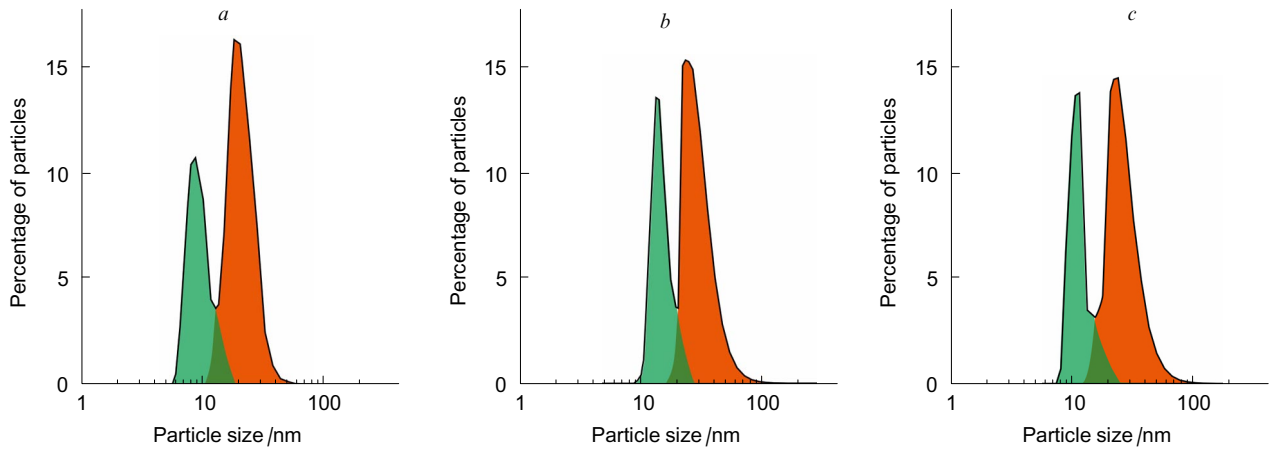


Figure 17. Bimodal nanoparticle size distributions for colloidal solutions of Ag_2S nanoparticles synthesized from reaction mixtures containing $AgNO_3$ (50 mmol litre^{-1}), Na_2S (24.5 mmol litre^{-1}) and Na_3Cit at Na_3Cit concentrations of 100 (*a*), 25 (*b*) and 12.5 mmol litre^{-1} (*c*).[122, 151]
The distribution maxima at ~7 – 15 nm and at 20 – 50 nm mainly correspond to Ag and Ag_2S nanoparticles, respectively.

DLS measurements of the particle size in the colloidal solutions synthesized from mixtures of aqueous solutions of $AgNO_3$ (50 mmol litre^{-1}) and Na_2S (24.5 mmol litre^{-1}) at Na_3Cit concentrations of 100, 25 and 12.5 mmol litre^{-1} revealed bimodal particle size and volume distributions (Fig. 17). It follows that these colloidal solutions contain two types of particles, namely, smaller and larger ones. Taking account of the TEM data for the Ag_2S/Ag heteronanostructures, one can assume that the smaller particles are silver, while the larger particles are Ag_2S. The silver particles are two to three times smaller in size than the Ag_2S particles; therefore, the volume of an Ag particle is about 10 – 20 times smaller than that of an Ag_2S particle. According to DLS data, the volume fraction of the small particles is much lower than that of the large particles; however, the number of the Ag particles is comparable with that of the Ag_2S particles owing to the small volume of the former.

This version of the method of hydrochemical bath deposition of Ag_2S/Ag heteronanostructures with controlled size of Ag_2S and Ag nanoparticles from aqueous solutions of $AgNO_3$, Na_2S and Na_3Cit was patented.[153]

5. Advantages and drawbacks of various methods for synthesis of nanostructured silver sulfide

The advantages and drawbacks of the main methods for the synthesis of various forms of nanostructured Ag_2S and heteronanostructures based on it have been analyzed[154] and summarized in Table 2.

Table 2. Methods for the synthesis of various forms of nanostructured silver sulfide.

Main reactants	Form of nanostructured Ag_2S	Advantages	Drawbacks	Ref.
		Hydrothermal synthesis		
$AgNO_3$, CS_2, Na_2S, NH_4OH, N_2H_4CS, $C_{19}H_{42}BrN$, $N_2S_2O_3$, $Ag[S_2P(OR)_2]$ (R = C_nH_{2n+1}), n-$C_{13}H_{25}SH$, PVP	Leaf-like nanosheets, nanocubes, hollow nanohexagons, tetrahedral and rice-shaped nanoparticles	Wide range of products	Complex processes and equipment, nonuniform nanoparticle size distribution, hazardous reactants	99, 101, 103, 104, 106
$AgNO_3$, Na_2S, $C_3H_6O_2S$, AcOH, NaOH	Quantum dots	Controlled small size and narrow quantum dot size distribution	Multistage process	121
		Solvothermal synthesis		
$AgNO_3$, CS_2, NH_4OH, EtOH, PVP	Flakes and star-shaped nanoparticles	Cheap reactants	Complex equipment, large nanoparticles, nonuniform nanoparticle size distribution, hazardous reactants	98
$AgNO_3$, n-$C_{18}H_{37}NH_2$	Ultralong nanowires	High aspect ratio, single-crystalline nanowires	Complex equipment	111
$AgNO_3$, $C_{13}H_{11}NS$, $C_{19}H_{42}BrN$, Bu^nOH	Nanospheres	Good reproducibility of synthesis	Complex equipment, nonuniform nanoparticle size distribution	118

Table 2 (continued).

Main reactants	Form of nanostructured Ag_2S	Advantages	Drawbacks	Ref.
		Solvothermal synthesis		
$C_{18}H_{31}AgO_2$, $C_{18}H_{32}O_2$, EtOH	Monodisperse nanoparticles	Small size, uniform nanoparticle size distribution	Complex equipment	119
		Hydrochemical bath deposition		
$AgNO_3$, NH_4OH, $Na_2S_2O_3$, N_2H_4CS	Rod-like nanocrystallites, nanowires, worm-like nanoparticles, nanopolyhedra	Simplicity, high yield, reproducible synthesis	Nonuniform nanoparticle size distribution	97, 100
$AgNO_3$, Na_2S, Na_3Cit or Trilon B	Nanoparticles, quantum dots	Wide range of products, controlled nanoparticle size, simple synthesis, safe reactants	Possible presence of metallic Ag impurity in Ag_2S	69, 70, 136,150
$AgNO_3$, Na_2S, Na_3Cit	Heteronanostructure	Controlled product size, safe reactants, safety	Low yield	150, 151
		Template synthesis		
$AgNO_3$, $C_4H_6O_2$, $Na_2S_2O_3$, $(NH_4)_2S_2O_6(O_2)$, n-heptane, $C_{19}H_{42}BrN$, CS_2	Microspheres with flower-like surface structure, hollow nanospheres	Controlled product size and morphology	Complex multistage process	102, 105
		Thermal decomposition (hot injection)		
C_7H_5AgOS, $C_{24}H_{51}P$, Et_2NCS_2Ag, silver xanthate	Nanocubes and nanospheres	Controlled size and morphology nanoparticles; simplicity, safe reactants	Complex equipment, multistage process	8, 93 – 95
		Pyrolysis		
$AgNO_3$, S, n-$C_{18}H_{35}NH_2$	Nanoparticles	Uniform nanoparticle size	Low yield	117
		Thermal decomposition		
Et_2NCS_2Ag, n-$C_{12}H_{25}SH$	Quantum dots	Controlled small size and narrow quantum dot size distribution	Complex multistage process	120
		Gas – solid reaction on Ag substrate		
Ag foil and $H_2S + O_2$ gas mixture (atmosphere)	Nanowires	High aspect ratio, single-crystalline nanowires	Complex equipment and process	109
		Template solvothermal synthesis with cation exchange		
S, $Cd(OAc)_2$, CuCl, $AgNO_3$, $(CH_2OH)_2$, anhydrous EtOH, $NH_2CH_2CH_2NH_2$	Nanowires	Controlled phase composition of nanowires	Complex equipment, multistage process	112,113
		Hydrothermal synthesis with cation exchange		
$AgNO_3$, Na_2S, Na_3Cit, $C_{18}H_{17}K_2O_8PS_2$	Heteronanostructure	Controlled heteronano-structure size	Complex process	9, 146
		Cation exchange		
$Cd(NO_3)_2$, $AgNO_3$, Na_3Cit, N_2H_4CS, EtOH C_3H_6O, PVP	Heteronanostructure	Controlled heteronano-structure size	Complex multistage process	25
		Laser ablation		
Ag, n-$C_{16}H_{33}NMe_3Br$, C_2H_5NS	Heteronanostructure	Controlled heteronano-structure size	Complex process, high cost	148

A comparison of methods for the synthesis of nanostructured silver sulfide revealed versatile character of the method of hydrochemical bath deposition. This approach allows one to synthesize colloidal solutions of Ag_2S nanoparticles, isolated Ag_2S nanoparticles and quantum dots with protective shell, heteronanostructures based on silver sulfide, as well as nanocrystalline and coarse-crystalline Ag_2S powders. All forms of nanostructured silver sulfide with controlled particle size can be obtained by varying the reactant concentrations in solution and the synthesis conditions. Preparation of colloidal solutions and deposition of silver sulfide powders without metallic Ag impurity requires the use of reaction mixtures with an excess concentration of Na_2S. An important advantage of hydrochemical bath deposition over other methods is utilization of environmentally safe reactants and the absence of hazardous substances among products. Yet another advantage is the reproducibility of results.

Both hydrothermal and solvothermal methods allow one to synthesize rather large silver sulfide particles of different morphology (nanosheets, flakes or star-shaped crystallites, faceted crystals, hollow particles, *etc.*) and size varied from hundreds of nanometres to tens of micrometres.

The most preferred method for the preparation of Ag_2S nanowires with a high aspect ratio is template synthesis using silver foil or alumina templates.

Being a versatile method, hydrochemical bath deposition can be used to synthesize all types of other nanostructured metal sulfides (Cd, Zn, Pb and Cu) by replacing the silver precursor by the desired metal precursor.

6. Applications of nanostructured silver sulfide

Main fields of application of nanostructured silver sulfide include micro- and nanoelectronics, biosensorics and catalysis.

An issue in present-day electronics is to develop nonvolatile memory devices. At present, the most widely used nonvolatile memory devices suitable for physical data transfer and(or) storage are compact USB flash drives rather than diskettes and CD-ROM. Progress in electronics is aimed to provide further miniaturization, improved performance and increased storage capacity of such devices.

High-performance atomic resistive switches are a promising type of nonvolatile memory devices; here, read/write operations are implemented involving ion exchange.[155, 156] In the case of cation migration, silver and silver sulfide heteronanostructures are most widely used.[17 – 21] The Ag_2S/Ag heteronanostructures combine the sulfide (semiconductor or ionic conductor depending on the structure) and silver (electronic conductor). Application of nanostructured silver sulfide for fabrication of heteronanostructures for nanoelectronics offers the greatest promise for this substance.

The operation of Ag_2S/Ag heteronanostructures as resistive switches is based on the phase transformation of acanthite α-Ag_2S (insulator) to argentite β-Ag_2S (superionic conductor). Transition to the high-conductivity state is due to abrupt disordering of the cation sublattice. The high-conductivity state of a crystal can be achieved by electric field induced 'melting' of the cation sublattice which occurs without heating of the crystal.[157, 158] Such a transformation of nanocrystalline silver sulfide under the action of external electric field was confirmed in a number of studies.[19 – 21, 145]

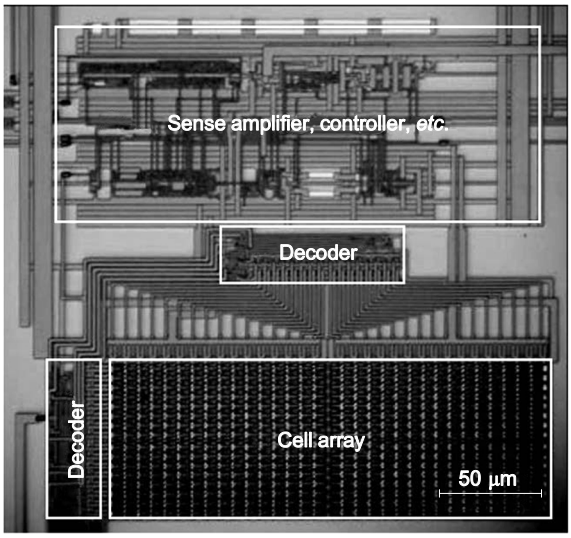


Figure 18. Two-input nonvolatile 1 kB memory device with atomic switches based on Ag_2S/Ag heteronanostructures.[159]

This allows the superionic state of silver sulfide to be achieved at room temperature, which offers great prospects for practical application of the material.

There is considerable literature on Ag_2S/Ag heteronanostructures and their application as resistive switches and nonvolatile memory devices. For instance, an Ag_2S/Ag heteronanostructure with a nanodot density of 10^{10} Gbit cm^{-2} (60 Gbit $inch^{-2}$) was fabricated on a silicon substrate.[147]

Besides, fabrication of Ag_2S/Ag heteronanostructures was followed by the design of switches and memory devices for new-generation electronics.[159 – 164] As an example, Fig. 18 presents a 1 kByte nonvolatile memory chip based on Ag_2S/Ag heteronanostructures that act as atomic switches.[161]

The operation of the Ag_2S/Ag resistive atomic switches is based on control of the motion of silver atoms and cations and reduction of the latter to form a conductive channel. Atomic switches are characterized by low power consumption, very low resistance and high performance. The unique operating mechanism of these devices makes it possible to develop various types of atomic switches (two- and three-terminal ones), which equates the atomic switching technology with such a versatile technology as the use of transistors as elements for memory and logic devices. Note that recent research activity in the field of fast switches for modern electronics led to emergence of a new investigation line called molecular switches.[165]

Design of fluorescent labels (biolabels, biomarkers) based on Ag_2S quantum dots for applications in biology and medicine seems to be quite promising.[26, 27, 166 – 171] The advantages of silver sulfide quantum dots over organic dyes include the possibility to control the luminescence wavelength, the high extinction coefficient, the solubility in various solvents, the stability of luminescence against environmental factors and high photostability. The photoluminescence brightness is much higher than that of conventional organic fluorescent dyes. The surface of Ag_2S quantum dots can be modified with various agents (see Fig. 11) that enable selective binding to biological objects. As an

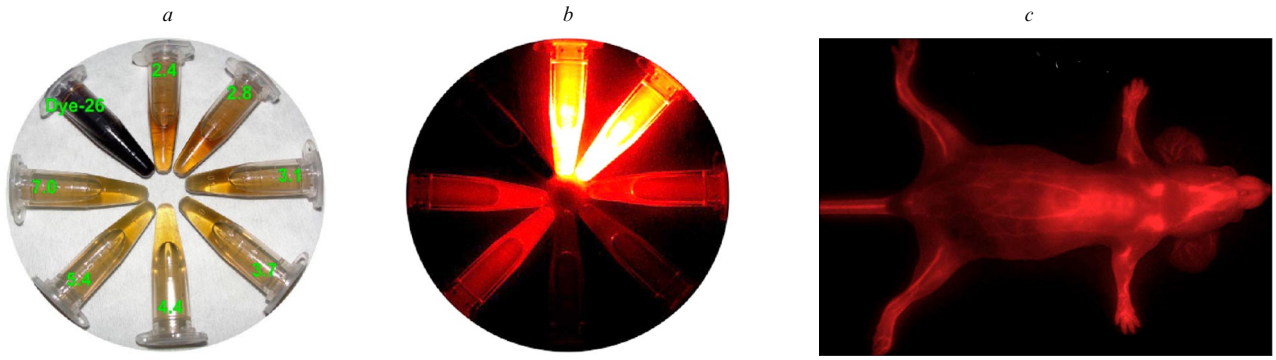


Figure 19. Daylight images of Ag_2S colloidal solutions (*a*) and their near-IR fluorescence at 808 nm (*b*)[171] and a fluorescent image of a mouse after i.v. injection of Ag_2S colloidal solution under irradiation at 808 nm (*c*).[27]
(*a*) Numbers denote the size of Ag_2S quantum dots (in nm); the Dye-26 solution is shown for comparison.

example, Fig. 19 presents the images of colloidal solutions containing Ag_2S quantum dots of different size, their near-IR fluorescence after excitation at 808 nm and a fluorescent image of a mouse after i.v. injection of a colloidal solution of water-soluble Ag_2S quantum dots that luminesce in the visible region.

The antibacterial activity of Ag_2S colloidal solutions, nanoparticles and Ag_2S-based heteronanostructures can be used for deactivation of various types of bacteria.[24, 25, 136, 168, 172] Unique optical properties of semiconductor Ag_2S quantum dots offer additional prospects for application in medicine, *e.g.*, in the design of optical sensors, fluorescent markers and photosensitizers.

Semiconductor nanomaterials are widely used in various photocatalytic processes. Nanostructured silver sulfide and heteronanostructures based on this substance are treated as promising materials for catalysis and photocatalysis.[9, 29, 131, 173 – 177] Monodisperse hybrid nanocomposites Ag_2S@Ag can be used for removal of organic pollutants, *e.g.*, Methyl Blue and Methyl Orange dyes from wastewater.[148]

Photocatalytic splitting of water in the presence of heterogeneous nanocrystalline photocatalysts[178] has been intensively studied as potential method for hydrogen production from water under solar irradiation. Hybrid nanostructures $Ag_{2-\delta}S/Ag$ possess improved photocatalytic properties since by varying the composition of the nonstoichiometric sulfide $Ag_{2-\delta}S$ ($\delta > 0$), one can control the optical properties of the composite materials and enhance their photocatalytic activity under the irradiation conditions.[131, 176] Emphasize that vacancies are also active sites for charge recombination.

Photocatalytic evolution of hydrogen over silver sulfide was studied taking aqueous solutions of $Na_2S - Na_2SO_3$ under irradiation with light at 450 nm as examples.[179, 180] Nonstoichiometric sulfide ($Ag_{1.93}S$) nanoparticles and Ag_2S/Ag heteronanostructures were synthesized by hydrochemical bath deposition. The highest hydrogen evolution was observed for the hybrid catalyst $Ag_{2-\delta}S/Ag$ consisting of nonstoichiometric sulfide $Ag_{1.93}S$ and metallic silver. The rate of hydrogen evolution was 2.04 ± 0.04 μmol h^{-1}, being nearly six times higher than in the experiments with a commercially available Degussa P25 TiO_2 catalyst (0.36 μmol h^{-1}) under identical conditions.[181] A scheme of molecular hydrogen evolution from aqueous solutions of $Na_2S - Na_2SO_3$ over $Ag_{2-\delta}S/Ag$ photocatalyst is shown in Fig. 20.

A detailed analysis of modern concepts of heterogeneous photocatalysts for molecular hydrogen production from water and aqueous solutions under visible-light and near-UV irradiation is available.[182] The emphasis was placed on the development and application of visible-light-responsive photocatalysts based on semiconductor sulfides.

Recently, nanostructured silver sulfide has also been considered as a promising thermoelectric material.[28] When

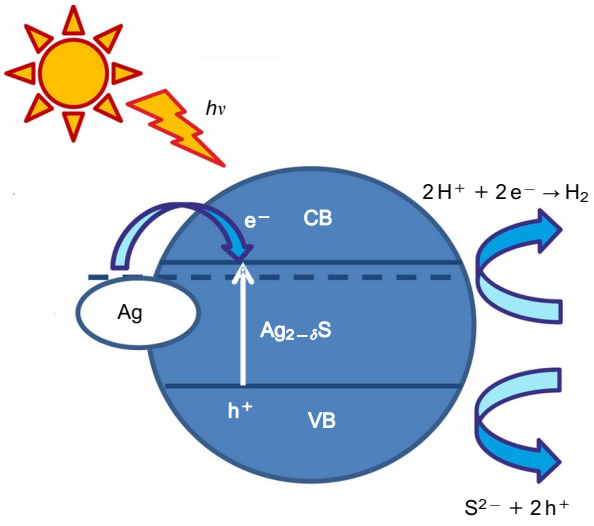


Figure 20. Molecular hydrogen evolution over $Ag_{2-\delta}S/Ag$ photocatalyst: a schematic.[179]
CB stands for conduction band and VB stands for valence band. Visible light excites electrons e^- in the conduction band of Ag nanoparticles, the electrons are transferred to the conduction band of $Ag_{2-\delta}S$ nanoparticles where H^+ ions are reduced and molecular hydrogen is thus formed. Simultaneously, photogenerated holes h^+ oxidize S^{2-} ions. Electron transfer between Ag and Ag_2S, *i.e.*, the presence of a heterojunction between Ag_2S nanoparticles and Ag, is the reason for enhanced evolution of hydrogen over Ag_2S/Ag photocatalyst compared to pure silver sulfide. The presence of vacancies in the metal sublattice of $Ag_{2-\delta}S$ (nonstoichiometry of silver sulfide) also favours the observed enhancement of photocatalytic activity of the Ag_2S/Ag photocatalyst.

two different semiconductors or a semiconductor and a conductor become in immediate contact, thermoelectric effects related to conversion of heat into electricity occur in the electric circuit. Semiconductor thermoelements are characterized by higher efficiency of heat conversion into electricity compared to metallic thermocouples. Silver sulfide is of interest as thermoelectric material owing to the reversible transition between the monoclinic semiconducting (α-Ag_2S) and cubic superionic (β-Ag_2S) phases. This allows the thermoelectric effect in Ag_2S to be realized near the phase transition temperature with silver sulfide acting as thermoelement. The efficiency of a thermoelectric material is characterized by its dimensionless figure of merit (ZT), defined as $ZT = \sigma S^2 T/\kappa$, where σ is the specific conductivity, S is the Seebeck coefficient, T is absolute temperature and κ is the specific thermal conductivity. The most efficient thermoelectrics have $ZT = 1.8 - 2.0$ and their efficiency in heat conversion into electricity is 15% – 20%.[183] In the experiments[28] with nanostructured Ag_2S (particle size $\sim$10 nm) the temperature dependences $\sigma(T)$, $\kappa(T)$ and $S(T)$ were optimized in such a manner that the maximum dimensionless figure of merit was observed just at the transition temperature. Since the Seebeck coefficient of a nanocrystalline Ag_2S film is -198 $\mu V\ K^{-1}$ at 400 K,[184] one can expect even greater dimensionless figure of merit for the nanofilm. It is believed[28] that joint contribution of the phase transition, small particle size and possibility of doping opens a new approach to the design of sulfide nanomaterials with optimum thermoelectric properties.

By and large, the properties of nanostructured silver sulfide imply a great potential of the material for practical applications.

7. Conclusion

Modern progress in science and technology is advanced by electronics as well as computer, bio- and nanotechnologies. In the last two decades, research into nanomaterials and nanotechnologies of semiconductor chalcogenides including sulfides has been most actively developed. Major efforts are aimed to develop methods for the synthesis of nanostructured sulfides with controlled geometry and morphology.

Interest in silver has sulfide has persisted for more than 150 years due to the potential of this compound for application in optoelectronics, power engineering, fabrication of hybrid nanocomposite materials, biology and medicine. A specific feature of coarse-crystalline silver sulfide compared to other sulfides is oxidative stability, *viz.*, heating in air causes dissociation of Ag_2S into metallic silver and sulfur rather than oxidation. This is also characteristic of nanostructured silver sulfide, although to a lesser extent, namely, heating of Ag_2S even in protective atmosphere or *in vacuo* can be accompanied by not only growth of nanoparticles, but also partial dissociation, oxidation of elemental sulfur and changes in the phase composition.

Materials presented in this review demonstrate that nanostructured silver sulfide can be synthesized using various methods. Nanostructured Ag_2S with specified properties can be synthesized using a method which provides control of nanoparticle size and surface protection. This can be done by, *e.g.*, the deposition from aqueous solutions which can give various forms of nanostructured silver sulfide. The synthesis in water excludes the influence of toxic organic ligands or toxic organic media on biological objects. One can expect that further progress in methods for the synthesis of Ag_2S nanoparticles with specified size and shape will extend the application of the material in optoelectronics, biology and medicine.

At the same time, certain issues in the hydrochemical synthesis of nanostructured silver sulfide are still to be solved.

Stable colloidal solutions contain the smallest Ag_2S nanoparticles (8 – 16 nm in size), but their concentration is very low (0.01 – 0.02 mg ml^{-1}). Therefore, an important problem in the synthesis of various forms of nanostructured silver sulfide is to prepare more saturated (concentrated) colloidal solutions with retention of long-term stability and small nanoparticle size.

Yet another topical issue is to obtain a narrow size distribution of nanoparticles, *i.e.*, to synthesize monodisperse nanoparticles. Indeed, the synthesis of monodisperse Ag_2S nanoparticles with a size scatter of at most 5% is of great importance because the properties of nanoparticles depend strongly on their size and degree of monodispersity. Prevenition of additional nucleation during the growth or, in other words, a complete separation of nucleation and growth is critical to successful synthesis of monodisperse nanoparticles without subsequent size separation.

Acceptance of the importance of these issues is a necessary step on the way to environmentally safe industrial-scale production of high-quality materials and devices based on nanostructured silver sulfide.

This review has been written with the financial support from the Russian Science Foundation (Project No. 14-23-00025).

Figures 2, 4, 6, 7, 9, 14, 16 and 17 are given with permission from John Wiley and Sons. Figure 3 is given with permission from Elsevier and the Royal Society of Chemistry. Figures 5, 10 – 13 and 20 are given with permission from Elsevier. Figure 15 is given with permission from Springer Nature. Figure 18 is given with permission from IEEE (Institute of Electrical and Electronics Engineers). Figure 19 is given with permission from American Chemical Society and Elsevier.

References

1. S.I.Sadovnikov, A.I.Gusev, A.A.Rempel. *Russ. Chem. Rev.*, **85**, 731 (2016)
2. X.Shi, S.Zheng, W.Gao, W.Wei, M.Chem, F.Deng, X.Liu, Q.Xiao. *J. Nanopart. Res.*, **16**, 2741 (2014)
3. S.Goel, F.Chen, W.Cai. *Small*, **10**, 631 (2013)
4. N.S.Kozhevnikova, A.S.Vorokh, A.A.Uritskaya. *Russ. Chem. Rev.*, **84**, 225 (2015)
5. A.K.Mahapatra, A.K.Dash. *Physica E*, **35**, 9 (2006)
6. A.Tang, Y.Wang, H.Ye, C.Zhou, C.Yang, X.Li, H.Peng, F.Zhang, Y.Hou, F.Teng. *Nanotechnology* **24**, 355602 (2013)
7. C.Cui, X.Li, J.Liu, Y.Hou, Y.Zhao, G.Zhong. *Nanoscale Res. Lett.*, **10**, 431 (2015)
8. W.P.Lim, Z.Zhang, H.Y.Low, W.S.Chin. *Angew. Chem., Int. Ed.*, **43**, 5685 (2004)
9. J.Yang, J.Y.Ying. *Angew. Chem., Int. Ed.*, **50**, 4637 (2011)
10. G.X.Zhu, Z.Xu. *J. Am. Chem. Soc.*, **133**, 148 (2011)
11. A.I.Kryukov, A.L.Stroyuk, N.N.Zin'chuk, A.V.Korzhak, S.Y.Kuchmii. *J. Mol. Catal. A: Chem.*, **221**, 209 **(**2004)
12. S.Shen, Y.Zhang, Y.Liu, L.Peng, X.Chen, Q.Wang. *Chem. Mater.*, **24**, 2407 (2012)
13. T.B.Nasrallah, H.Dlala, M.Amlouk, S.Belgacem, J.C.Bernede. *Synth. Met.*, **151**, 225 (2005)

14. T-Y.Hsu, H.Buhay, N.P.Murarka. In *Millimeter Optics*. (Ed. G.A.Tanton). *SPIE Proc*., **259**, 38 (1980)
15. D.Karashanova, D.Nihtianova, K.Starbova, N.Starbov. *Solid State Ionics*, **171**, 269 (2004)
16. L.Liu, S.Hu, Y.-P.Dou, T.Liu, J.Lin, Y.Wang. *Beilstein J. Nanotechnol*., **6**, 1781 (2015)
17. C.H.Liang, K.Terabe, T.Hasegawa, R.Negishi, T.Tamura, M.Aono. *Small*, **1**, 971 (2005)
18. C.H.Liang, K.Terabe, T.Hasegawa, M.Aono. *Nanotechnology*, **18**, 485202 (2007)
19. M.Morales-Masis, S.J.Molen, W.T.Fu, M.B.Hesselberth, J.M.Ruitenbeek. *Nanotechnology*, **20**, 095710 (2009)
20. Z.Xu, Y.Bando, W.Wang, X.Bai, D.Golberg. *ACS Nano*, **4**, 2515 (2010)
21. A.N.Belov, O.V.Pyatilova, M.I.Vorobiev. *Adv. Nanopart*., **3**, 1 (2014)
22. M.M.El-Nahass, A.A.M.Farag, E.M.Ibrahim, S.Abd-El-Rahman. *Vacuum*, **72**, 453 (2004)
23. U.M.Jadhav, S.N.Patel, R.S.Patil. *Res. J. Chem. Sci.*, **3** (7), 69 (2013)
24. M.L.Pang, J.Y.Hu, H.C.Zeng. *J. Am. Chem. Soc*., **132**, 10771 (2010)
25. S.Xiong, B.Xi, K.Zhang, Y.Chen, J.Jiang, J.Hu, H.C.Zeng. *Sci. Rep*., **3**, 2177 (2013)
26. P.Jiang, C.-N.Zhu, Z.-L.Zhang, Z.-Q.Tian, D.-W.Pang. *Biomaterials*, **33**, 5130 (2012)
27. C.Li, Y.Zhang, M.Wang, Y.Zhang, G.Chen, L.Li, D.Wu, Q.Wang. *Biomaterials*, **35**, 393 (2014)
28. C.Xiao, J.Xu, K.Li, J.Feng, J.Yang, Y.Xie. *J. Am. Chem. Soc*., **134**, 4287 (2012)
29. A.Eftekhari, V.J.Babu, S.S.Ramakrishna. *Int. J. Hydr. Energy*, **42**, 11078 (2017)
30. A.A.Rempel. *Russ. Chem. Rev*., **76**, 435 (2007)
31. *Nanomaterials: Synthesis, Properties and Applications*. (Eds A.S.Edelstein, R.C.Cammarata). (Bristol: IOP, 1996)
32. A.I.Gusev. *Physics – Uspekhi*, **41**, 49 (1998)
33. H.Gleiter. *Acta Mater*., **48**, 1 (2000)
34. *Slovar' Nanotekhnologicheskikh i Svyazannykh s Nanotekhnologiyami Terminov*. (Dictionary of Nanotechnology and Nanotechnology-Related Terms). (Ed. S.V.Kolyuzhnyi) (Moscow: Fizmatlit, 2010)
35. A.I.Gusev, A.A.Rempel. *Nanokristallicheskie Matrialy*. (Nanocrystalline Materials). (Moscow: Fizmatlit, 2000)
36. A.I.Gusev, A.A.Rempel. *Nanocrystalline Materials*. (Cambridge: Cambridge Int. Sci. Publ., 2004)
37. A.I.Gusev. *Nanomaterialy, Nanostruktury, Nanotekhnologii*. (Nanomaterials, Nanostructures and Nanotechnologies) (Moscow: Fizmatlit, 2009)
38. H.-E.Schaefer. *Nanoscience. The Science of the Small in Physics, Engineering, Chemistry, Biology and Medicine*. (Heidelberg, Dordrecht, New York: Springer, 2010)
39. R.F.Khairutdinov. *Russ. Chem. Rev*., **67**, 109 (1998)
40. Zh.I.Alferov. *Rev. Mod. Phys*., **73**, 767 (2001)
41. A.P.Alivisatos. *Science*, **271**, 933 (1996)
42. N.N.Ledentsov, V.M.Ustinov, V.A.Shchukin, P.S.Kop'ev, Zh.I.Alferov, D.Bimberg. *Semiconductors*, **32**, 343 (1998)
43. T.Theivasanthi, M.Alagar. *Res. Appl. Mater*., **1**, 36 (2013)
44. S.I.Sadovnikov, A.I.Gusev. *J. Therm. Anal. Color*., **131**, 1155 (2018)
45. R.C.Sharma, Y.A.Chang. *Bull. Alloy Phase Diagrams*, **7**, 263 (1986)
46. H.Rau. *J. Phys. Chem. Solids*, **35**, 1553 (1974)
47. G.Bonnecaze, A.Lichanot, S.Gromb. *J. Phys. Chem. Solids*, **39**, 299 (1978)
48. H.Reye. *Z. Phys. Chem. Neue Folge*, **119**, 251 (1980)
49. M.K.van Doorselaer. *J. Photograph. Sci*., **35**, 42 (1987)
50. A.J.Frueh. *Z. Kristallogr*., **110**, 136 (1958)
51. R.Sadanaga, S.Sueno. *Mineral. J. Jpn*., **5**, 124 (1967)
52. P.Rahlfs. *Z. Phys. Chem. B*, **31**, 157 (1936)
53. R.J.Cava, F.Reidinger, B.J.Wuensch. *J. Solid State Chem*., **31**, 69 (1980)
54. T.Blanton, S.Misture, N.Dontula, S.Zdzieszynski. *Powder Diffract*., **26**, 114 (2011)
55. A.J.Frueh. *Am. Mineral*., **46**, 654 (1961)
56. S.I.Sadovnikov, A.I.Gusev, A.A.Rempel. *Superlat. Microstruct*., **83**, 35 (2015)
57. S.I.Sadovnikov, A.I.Gusev, A.A.Rempel. *Phys. Chem. Chem. Phys*., **17**, 20495 (2015)
58. S.I.Sadovnikov, A.I.Gusev, A.A.Rempel. *Rev. Adv. Mater. Sci*., **41**, 7 (2015)
59. S.I.Sadovnikov, A.I.Gusev, A.V.Chukin, A.A.Rempel. *Phys. Chem. Chem. Phys*., **18**, 4617 (2016)
60. S.I.Sadovnikov, A.V.Chukin, A.A.Rempel, A.I.Gusev. *Phys. Solid State*, **58**, 30 (2016)
61. B.Kim, C.-S.Park, M.Murayama, M.F.Hochella. *Environ. Sci. Technol*., **44**, 7509 (2010)
62. L.Han, Y.Lv, A.M.Asiri, A.O.Al-Youbi, B.Tu, D.Y.Zhao. *J. Mater. Chem*., **22**, 7274 (2012)
63. S.I.Sadovnikov, A.I.Gusev, A.A.Rempel. *Phys. Chem. Chem. Phys*., **17**, 12466 (2015)
64. S.I.Sadovnikov, A.I.Gusev, A.A.Rempel. *Dokl. Phys. Chem.,* **464**, 238 (2015)
65. P.Junod. *Helv. Phys. Acta*, **32**, 567 (1959)
66. P.Junod, H.Hediger, B.Kilchör, J.Wullschleger. *Philos. Mag*., **36**, 941 (1977)
67. S.H.Ehrlich. *J. Imaging Sci. Technol*., **37**, 73 (1993)
68. J.Jang, K.Cho, S.H.Lee, S.Kim. *Mater. Lett*., **62**, 1438 (2008)
69. S.I.Sadovnikov, A.A.Rempel. *Inorg. Mater*., **51**, 759 (2015)
70. S.I.Sadovnikov, A.I.Gusev, E.Yu.Gerasimov, A.A.Rempel. *Chem. Phys. Lett*., **642**, 17 (2015)
71. R.Chen, N.T.Nuhfer, L.Moussa, H.R.Morris, P.M.Whitmore. *Nanotechnology*, **19**, 455604 (2008)
72. W.Zhang, L.Zhang, Z.Hui, X.Zhang, Y.Qian. *Solid State Ionics*, **130**, 111 **(**2000)
73. X.F.Qian, J.Yin, J.C.Huang, Y.F.Yang, X.X.Guo, Z.K.Zhu. *Mater. Chem. Phys*., **68**, 95 (2001)
74. X.F.Qian, J.Yin, S.Feng, S.H.Liu, Z.K.Zhu. *J. Mater. Chem*., **11**, 2504 (2001)
75. X.Lu, L.Li, W.Zhang, C.Wang. *Nanotechnology*, **16**, 2233 (2005)
76. V.B.Prabhune, N.S.Shinde, V.J.Fulari. *Appl. Surf. Sci*., **255**, 1819 (2008)
77. P.Jiang, Z.-Q.Tian, C.-N.Zhu, Z.-L.Zhang, D.-W.Pang. *Chem. Mater*., **24**, 3 (2011)
78. H.Meherzi-Maghraoui, M.Dachraoui, S.Belgacem, K.D.Buhre, R.Kunst, P.Cowache, D.Lincot. *Thin Solid Films*, **288**, 217 **(**1996)
79. S.S.Dhumure, C.D.Lokhande. *Mater. Chem. Phys*., **28**, 141 (1991)
80. L.-M.Lyu, M.H.Huang. *Chem. – Asian J*., **8**, 1847 **(**2013)
81. M.Lismont, C.A.Paez, L.Dreesen. *J. Colloid Interface Sci*., **447**, 40 (2015)
82. Z.Li, L.Jia, Y.Li, T.He, X.-M.Li. *Appl. Surf. Sci*., **345**, 122 (2015)
83. X.Gao, Y.Cui, R.M.Levenson, L.W.K.Chung, S.Nie. *Nat. Biotechnol*., **22**, 969 (2004)
84. J.Xiang, H.Cao, Q.Wu, S.Zhang, X.Zhang, A.A.R.Watt. *J. Phys. Chem. C*, **112**, 3580 (2008)
85. Y.Yu, K.Zhang, S.Sun. *Appl. Surf. Sci*., **258**, 7181 (2012)
86. J.Zeng, Y.Zheng, M.Rycenga, J.Tao, Z.Y.Li, Q.Zhang, Y.Zhu, Y.Xia. *J. Am. Chem. Soc*., **132**, 8552 (2010)
87. L.Gutierrez, C.Aubry, M.Cornejo, J.-P.Croue. *Langmuir*, **31**, 8865 (2015)
88. S.D'Souza, P.Mashazi, J.Britton, T.Nyokong. *Polyhedron*, **99**, 112 (2015)
89. R.Mendoza-Reséndez, A.Gómez-Treviño, E.D.Barriga-Castro, N.O.Núñez, C.Luna. *RSC Adv*., **4**, 1650 (2014)

90. D.Ayodhya, G.Veerabhadram. *J. Photochem. Photobiol., B*, **157**, 57 (2016)
91. H.-Y.Yang, Y.-W.Zhao, Z.-Y.Zhang, H.-M.Xiong, S.-N.Yu. *Nanotechnology*, **24**, 055706 (2013)
92. A.C.C.Esteves, T.Trindade. *Curr. Opin. Solid State Mater. Sci.*, **6**, 347 (2002)
93. Q.Tang, S.M.Yoon, H.J.Yang, Y.Lee, H.J.Song, H.R.Byon, H.C.Choi. *Langmuir*, **22**, 2802 (2006)
94. T.X.Wang, H.Xiao, Y.C.Zhang. *Mater. Lett.*, **62**, 3736 (2008)
95. C.L.Zhang, S.M.Zhang, L.G.Yu, Z.J.Zhang. *Mater. Lett.*, **85**, 77 (2012)
96. C.Burda, X.B.Chen, R.Narayanan, E.I.Sayed. *Chem. Rev.*, **105**, 1025 (2005)
97. Y.Zhao, D.W.Zhang, W.F.Shi. *Mater. Lett.*, **61**, 3232 (2007)
98. C.G.Xu, Z.C.Zhang, Q.Ye. *Mater. Lett.*, **58**, 1671 (2004)
99. M.H.Chen, L.Gao. *Mater. Lett.*, **60**, 1059 (2006)
100. H.J.Zhai, H.S.Wang. *Mater. Res. Bull.*, **43**, 2354 (2008)
101. X.B.Wang, W.M.Liu, J.C.Hao, X.G.Fu, B.S.Xu. *Chem. Lett.*, **34**, 1664 (2005)
102. Y.Fang, C.Bai, Y.Zhang. *Chem. Commun.*, 804 (2004)
103. Y.Z.Sun, B.B.Zhou. *Mater. Lett.*, **64**, 1347 (2010)
104. Z.Zhuang, Q.Peng, X.Wang, Y.Li. *Angew. Chem., Int. Ed.*, **46**, 8174 (2007)
105. R.G.Chaudhuri, S.Paria. *J. Colloid. Interface Sci.*, **369**, 117 (2012)
106. L.Y.Lv, H.Wang. *Mater. Lett.*, **121**, 105 (2014)
107. Yu.A.Popov. *Teoriya Vzaimodeistviya Metallov i Splavov s Korrozionno-Aktivnoi Sredoi*. (Theory of Interaction of Metals and Alloys with a Corrosive Environment) (Moscow: Nauka, 1995)
108. S.I.Sadovnikov, A.I.Gusev. *J. Mater. Chem., A*, **5**, 20289 (2017)
109. X.Wen, S.Wang, Y.Xie, X.-Y.Li, S.Yang. *J. Phys. Chem. B*, **109**, 10100 (2005)
110. S.C.Yan, H.T.Wang, Y.P.Zhang, S.C.Li, Z.D.Xiao. *J. Non-Cryst. Solids*, **354**, 5559 (2008)
111. D.Wang, C.Hao, W.Zheng, Q.Peng, T.Wang, Z.Liao, D.Yu, Y.Li. *Adv. Mater.*, **20**, 2628 (2008)
112. S.Yan, K.Shen, X.Xu, Y.Shi, J.Wu, Z.Xiao. *Synth. Met.*, **161**, 1646 (2011)
113. C.-S.Tan, C.-H.Hsiao, S.-C.Wang, P.-H.Liu, M.-Y.Lu, M.H.Huang, H.Ouyang, L.-J.Chen. *ACS Nano*, **8**, 9422 (2014)
114. J.Chen, T.Zhang, L.L.Feng, M.Zhang, X.Zhang, H.Su, D.Cui. *Mater. Lett.*, **96**, 224 (2013)
115. C.Siva, C.N.Iswarya, P.Baraneedharan, M.Sivakumar. *Mater. Lett.*, **134**, 56 (2014)
116. M.Koneswaran, R.Narayanaswamy. *Sens. Actuators, B*, **139**, 104 (2009)
117. X.M.Hou, X.L.Zhang, W.Yang, Y.Liu. *Mater. Res. Bull.*, **47**, 2579 (2012)
118. M.Shakouri-Arani, M.Salavati-Niasari. *Spectrochim. Acta, Part A*, **133**, 463 (2014)
119. X.Wang, J.Zhuang, Q.Peng, Y.D.Li. *Nature (London)*, **437**, 121 (2005)
120. Y.Zhang, G.Hong, Y.Zhang, G.Chen, F.Li, H.Dai, Q.Wang. *ACS Nano*, **6**, 3695 (2012)
121. I.Hocaoglu, M.N.Çizmeciyan, R.Erdem, C.Ozen, A.Kurt, A.Sennaroglu, H.Y.Acar. *J. Mater. Chem.*, **22**, 14674 (2012)
122. S.I.Sadovnikov, A.I Gusev. *Eur. J. Inorg. Chem.*, 4944 (2016)
123. P.Anastas, N.Eghbali. *Chem. Soc. Rev.*, **39**, 301 (2010)
124. P.Patnaik. *Dean's Analytical Chemistry Handbook*. (2nd Edn.). (New York: McGraw-Hill, 2004). Table 4.2
125. P.C.Lee, D.Meisel. *J. Phys. Chem.*, **86**, 3391 (1982)
126. *Gatan Misroscopy Suite*. Gatan Inc. Version 2.31.734.0. http://www.gatan.com/products/tem-analysis/gatan-microscopysuite-software
127. I.Martina, R.Wiesinger, D.Jembrih-Simbürger, M.Schreiner. *E-Preserv. Sci.: Morana RTD*, **9**, 1 (2012)
128. G.Socrates. *Infrared and Raman Characteristic Group Frequencies: Tables and Charts*. (3rd Edn.). (Chichester, New York: Wiley, 2001)
129. J.I.Lee, S.M.Howard, J.J.Kellar, K.N.Han, W.Cross. *Metall. Mater. Trans. B*, **32**, 895 (2001)
130. Y.Delgado-Beleño, M.Cortez-Valadez, C.E.Martinez-Nuñez, R.Britto Hurtado, A.B.Alvarez Ramón, O.Rocha-Rocha, H.Arizpe-Chávez, A.Perez-Rodríguez, M.Flores-Acosta. *Chem. Phys.*, **463**, 106 (2015)
131. W.Yang, L.Zhang, Y.Hu, Y.Zhong, H.B.Wu, X.W.Lou. *Angew. Chem., Int. Ed.*, **51**, 11501 (2012)
132. Patent RF 2572421; *Bull. Izobret.*, (2) (2016)
133. G.Hodes. *Chemical Solution Deposition of Semiconductor Films*. (New York: Marcel Dekker, 2002)
134. D.Vollath. *Nanomaterials: an Introduction to Synthesis, Properties and Applications*. (2nd Edn.). (Weinheim: Wiley-VCH, 2013)
135. T.V.Vinogradova, I.A.Glukhova, L.N.Maskaeva, V.F.Markov. *Eur. Rev. Chem. Res.*, **10**, 122 (2016)
136. S.I.Sadovnikov, Yu.V.Kuznetsova, A.A.Rempel. *Nanostruct. Nano-Objects.*, 7, 81 (2016)
137. S.I.Sadovnikov, A.A.Rempel, A.I.Gusev. *Nanostructured Lead, Cadmium and Silver Sulfides: Structure, Nonstoichiometry and Properties*. (Cham, Heidelberg: Springer, 2018)
138. Patent RF 2600761; *Bull. Izobret.*, (30) (2016)
139. N.S.Kozhevnikova, A.S.Vorokh, E.V.Shalaeva, I.V.Baklanova, A.P.Tyutyunnik, V.G.Zubkov, A.A.Yushkov, V.Yu.Kolosov. *J. Alloys Compd.*, **712**, 418 (2017)
140. Yu.V.Kuznetsova, S.V.Rempel, I.D.Popov, E.Yu.Gerasimov, A.A.Rempel. *Colloids Surf., A*, **520**, 369 (2017)
141. S.I.Sadovnikov, A.I.Gusev, E.Yu.Gerasimov, A.A.Rempel. *Inorg. Mater.*, **52**, 441 (2016)
142. Patent RF 2603666; *Bull. Isobret.*, (33) (2016)
143. J.Yang, E.H.Sargent, S.O.Kelley, J.Y.Ying. *Nat. Mater.*, **8**, 683 (2009)
144. K.Terabe, T.Hasegawa, T.Nakayama, M.Aono. *Nature (London)*, **433**, 47 (2005)
145. D.Wang, L.Liu, Y.Kim, Z.Huang, D.Pantel, D.Hesse, M.Alexe. *Appl. Phys. Lett.*, **98**, 243109 (2011)
146. J.Yang, J.Y.Lee, J.Y.Ying. *Chem. Soc. Rev.*, **40**, 1672 (2011)
147. H.Tanaka, T.Akai, D.Tanaka, T.Ogawa. *e-J. Surf. Sci. Nanotechnol.*, **12**, 185 (2014)
148. H.Zhang, M.Chen, D.M.Wang, L.Xu, X.D.Liu. *Opt. Mater. Express*, **6**, 2573 (2016)
149. A.I.Gusev, S.I.Sadovnikov. *Semiconductors*, **50**, 682 (2016)
150. S.I.Sadovnikov, A.I.Gusev. *J. Nanopart. Res.*, **18**, 277 (2016)
151. S.I.Sadovnikov, A.I.Gusev. *Biointerface Res. Appl. Chem.*, **6**, 1797 (2016)
152. A.I.Gusev, S.I.Sadovnikov. *Mater. Lett.*, **188**, 351 (2017)
153. Patent RF 2637710; *Bull. Izobret.*, (34) (2017)
154. S.I.Sadovnikov, A.I.Gusev. *J. Mater. Chem. A*, **5**, 17676 (2017)
155. M.N.Kozicki, M.Yun, S.-J.Yang, J.P.Aberouette, J.P.Bird. *Superlatt. Microstruct.*, **27**, 485 (2000)
156. T.Hasegawa, K.Terabe, T.Tsuruoka, M.Aono. *Adv. Mater.*, **24**, 252 (2012)
157. Yu.I.Kharkats *Fiz. Tv. Tela*, **23**, 2190 (1981)
158. Yu.Ya.Gurevich, Yu.I.Kharkats. *Sov. Phys. Uspekhi*, **25**, 257 (1982)
159. S.Kaeriyama, T.Sakamoto, H.Sunamura, M.Mizuno, H.Kawaura, T.Hasegawa, K.Terabe, T.Nakayama, M.Aono. *IEEE J. Solid-State Circuits*, **40**, 168 (2005)
160. A.Nayak, T.Tamura, T.Tsuruoka, K.Terabe, S.Hosaka, T.Hasegawa, M.Aono. *J. Phys. Chem. Lett.*, **1**, 604 (2010)

161. T.Hino, T.Hasegawa, K.Terabe, T.Tsuruoka, A.Nayak, T.Ohno, M.Aono. *Sci. Technol. Adv. Mater*., **12**, 013003 (2011)
162. T.Ohno, T.Hasegawa, A.Nayak, T.Tsuruoka, J.K.Gimzewski, M.Aono. *Appl. Phys. Lett*., **99**, 203108 (2011)
163. R.Gui, J.Sun, D.Liu, Y.Wang, H.Jin. *Dalton Trans*., **43**, 16690 (2014)
164. A.Gubicza, M.Csontos, A.Halbrittera, G.Mihaly. *Nanoscale*, **7**, 4394 (2015)
165. M.F.Budyka. *Russ. Chem. Rev*., **86**, 181 (2017)
166. C.Lutz, T.Hasegawa, T.Chikyow. *Nanoscale*, **8**, 14031 (2016)
167. X.Gao, S.Nie. *Anal. Chem*., **76**, 2406 (2004)
168. X.Ma, Y.Zhao, X.Jiang, W.Liu, S.Liu, Z.Tang. *ChemPhysChem*, **13**, 2531 (2012)
169. Y.Liu, L.Zhao, Jin.Zhang, Jinzha.Zhang, W.Zhao, C.Mao. *Talanta*, **161**, 87 (2016)
170. X.Zhang, Y.Gu, H.Chen. *J. Innov. Opt. Health Sci*., **7**, 1350059 (2014)
171. Y.Zhang, Y.Liu, C.Li, X.Chen, Q.Wang. *J. Phys. Chem. C*, **118**, 4918 (2014)
172. X.Chen, L.Ding, P.Liu, Q.Wang. *Surf. Interface Anal*., **46**, 301 (2014)
173. M.Basu, R.Nazir, C.Mahala, P.Fageria, S.Chaudhary, S.Gangopadhyay, S.Pande. *Langmuir*, **33**, 3178 (2017)
174. K.Nagasuna, T.Akita, M.Fujishima, H.Tada. *Langmuir*, **27**, 7294 (2011)
175. E.S.Aazam. *J. Ind. Eng. Chem*., **20**, 4033 (2014)
176. P.Chang, H.Cheng, W.Lin, X.Li, F.Zhao. *Chin. J. Catal*., **36**, 564 (2015)
177. D.Zhang, G.Xu, F.Chen. *Appl. Surf. Sci*., **351**, 962 (2015)
178. D.V.Markovskaya, S.V.Cherepanova, A.A.Saraev, E.Yu.Gerasimov, E.A.Kozlova. *Chem. Eng. J*., **262**, 146 (2015)
179. S.I.Sadovnikov, E.A.Kozlova, E.Yu.Gerasimov, A.A.Rempel. *Catal. Commun*., **100**, 178 (2017)
180. S.I.Sadovnikov, E.A.Kozlova, E.Yu.Gerasimov, A.A.Rempel, A.I.Gusev. *Int. J. Hydr. Energy*, **42**, 25258 (2017)
181. E.A.Kozlova, A.Yu.Kurenkova, V.S.Semeykina, E.V.Parkhomchuk, S.V.Cherepanova, E.Yu.Gerasimov, A.A.Saraev, V.V.Kaichev, V.N.Parmon. *ChemCatChem*, **7**, 4108 (2015)
182. E.A.Kozlova, V.N.Parmon. *Russ. Chem. Rev*., **86**, 870 (2017)
183. X.Zhang, L.-D.Zhao. *J. Materiomics*, **1**, 92 (2015)
184. M.Adelifard, R.Torkamani. *J Mater. Sci: Mater. Electron*., **26**, 7554 (2015)